

A search for rapid photometric variability in symbiotic binaries

J. L. Sokoloski,¹ Lars Bildsten,² and Wynn C. G. Ho³

¹*Department of Physics and Astronomy, Southampton University, Highfield, Southampton SO17 1BJ, UK*

²*Institute for Theoretical Physics and Department of Physics, Kohn Hall, University of California, Santa Barbara, CA 93106*

³*Center for Radiophysics and Space Research, Department of Astronomy, Cornell University, Ithaca, NY 14853*

Accepted . Received; in original form

ABSTRACT

We report on our survey for rapid (time scale of minutes) photometric variability in symbiotic binaries. These binaries are becoming an increasingly important place to study accretion onto white dwarfs since they are candidate Type Ia supernovae progenitors. Unlike in most cataclysmic variables, the white dwarfs in symbiotics typically accrete from a wind, at rates greater than or equal to $10^{-9}M_{\odot} \text{ yr}^{-1}$. In order to elucidate the differences between symbiotics and other white dwarf accretors, as well as search for magnetism in symbiotic white dwarfs, we have studied 35 symbiotic binaries via differential optical photometry. Included in our sample are all but one of the symbiotics from the lists of Kenyon (1986) and Downes & Keyes (1988) with published V magnitude less than 14 and declination greater than -20° . Our study is the most comprehensive to date of rapid variability in symbiotic binaries. We have found one magnetic accretor, Z And, previously reported by Sokoloski & Bildsten (1999). In four systems (EG And, BX Mon, CM Aql, and BF Cyg), some evidence for flickering at a low level (roughly 10 mmag) is seen for the first time. These detections are, however, marginal. For 25 systems, we place tight upper limits on both aperiodic variability (flickering) and periodic variability, highlighting a major difference between symbiotics and cataclysmic variables. The remaining five of the objects included in our sample (the 2 recurrent novae RS Oph and T CrB, plus CH Cyg, α Ceti, and MWC 560) had previous detections of optical flickering. We discuss our extensive observations of these previously-known flickering systems in a separate paper. Five new variable stars were discovered serendipitously in the fields of the survey objects, and the observations of these stars are also presented elsewhere. We discuss the impact of our results on the “standard” picture of wind-fed accretion, and speculate on the possibility that light from quasi-steady nuclear burning on the surface of the white dwarf hides the fluctuating emission from accretion.

Key words: accretion, accretion discs — methods: data analysis — surveys — binaries: symbiotic — stars: magnetic fields — stars: oscillations

1 INTRODUCTION

Symbiotic stars, or symbiotic systems (SS), are wide binaries in which material is transferred from an evolved red giant star to either a white dwarf (WD), main-sequence star, or in a few cases, a neutron star (Kenyon 1986). The material can be transferred either as the red giant overflows its Roche lobe, or by Bondi-Hoyle capture of the red-giant wind (see Yungelson et al. 1995 for modeling and population synthesis analysis of wind-fed SS). In most symbiotics, Bondi-Hoyle capture of the red-giant wind by the WD is the mode of mass transfer (Iben & Tutukov 1996; Luthardt 1992). Ra-

diation from the hot component turns the red-giant wind into a partially ionized nebula, producing the characteristic “symbiotic” optical spectrum with high ionization state emission lines superimposed on the cool red-giant continuum (Kenyon 1986).

Since most SS contain white dwarfs (sometimes in a state similar to white dwarfs at the centers of planetary nebulae; Kenyon & Webbink 1984; Mürset et al. 1991), it is important to place symbiotics within the context of other binaries with accreting white dwarfs. Selected properties of several types of accreting-WD systems — cataclysmic variables (CVs), supersoft X-ray sources, and symbiotics — are

arXiv:astro-ph/0104031v1 2 Apr 2001

listed in Table 1. It is clear that the three types of systems form a hierarchy of time scales, sizes, and accretion rates. Our survey for rapid variability in symbiotics represents part of an attempt to understand some of the phenomenological differences between symbiotics and the other WD accretors.

The mass-donor stars in CVs are low-mass main sequence stars which over-flow their Roche lobes. For CVs with orbital periods shorter than 2 hours, the time-averaged accretion rate of $\sim 10^{-10} M_{\odot} \text{ yr}^{-1}$ is set by gravitational radiation losses. For CVs with orbital periods in excess of 3 hours, where magnetic winds are presumably driving angular momentum losses (Warner 1995), the time-averaged accretion rate is larger by nearly an order of magnitude. These CV-accretion rates are too low for thermally-stable steady burning of the accreting fuel, and so this fuel is burned explosively in classical novae outbursts. In the classical supersoft X-ray sources, on the other hand, unstable mass transfer from an evolved main sequence star with mass in excess of a solar mass leads to accretion onto the WD at rates set by the Kelvin-Helmholtz time, $\dot{M} \sim 10^{-8} - 10^{-6} M_{\odot} \text{ yr}^{-1}$ (Kahabkha & van den Heuvel 1997). These rates are high enough for stable burning of the accreting fuel (van den Heuvel et al. 1992). Thus, the long-term optical variations seen in supersoft sources must be due to something other than a thermonuclear runaway, such as a change in the size of the WD photosphere in response to a change in the accretion rate (e.g. as in the system RX J0513.9-6951; Kahabkha & van den Heuvel 1997). In symbiotics, Bondi-Hoyle capture of the red giant wind gives $\dot{M} \sim 10^{-8} M_{\odot} \text{ yr}^{-1}$ onto the white dwarf, which could produce steady nuclear burning in some systems (Sion & Starrfield 1994).

There are at least 3 kinds of outbursting symbiotics. Symbiotic slow novae (or just ‘symbiotic novae’) have experienced a single, decades-long thermonuclear event. Recurrent novae have experienced multiple events of much shorter duration that are most likely of thermonuclear origin (Mikołajewska & Kenyon 1992b). Most symbiotics, however, show smaller ‘classical symbiotic outbursts’ whose origin is unclear. These classical symbiotic outbursts could be related to the quasi-steady burning of material on the surface of the WD, shell flashes, or unstable accretion. Symbiotics can also be divided into several sub-categories based upon their infrared (IR) colors. S-type, or ‘stellar’ systems have IR colors like those of isolated field red giants, whereas D-type, or ‘dusty’ systems have redder IR colors indicative of dust. The IR D-type systems generally contain Mira variables with very high mass loss rates, and are detectable radio sources (Seaquist & Taylor 1990). IR S-types usually have smaller binary separations than IR D-types, lower rates of mass-loss from the red giant, and fewer are detected in the radio (Seaquist & Taylor 1990). The S-types are more common, with about 80% of symbiotics falling into this category. Most of the results that will be presented in this paper are for IR S-type systems that have either classical symbiotic outbursts or no recorded outbursts.

1.1 Flickering as a Diagnostic of Nuclear Burning

As mentioned above, the different accretion rates in CVs and supersoft sources cause the fuel on a CV WD to be burned unstably in a nova explosion, whereas the fuel in at least some supersoft sources appears to be burned quasi-steadily

(van den Heuvel et al. 1992). The mass transfer rates in symbiotic systems bridge the gap between those in CVs and those in supersoft sources, and the thermal stability of the nuclear burning on the WDs in SS is still an open issue. The question of nuclear burning in classical symbiotics is important because the outbursts in these systems could be caused by processes related to the burning, and also because quasi-steady burning could allow the white dwarf to increase in mass until it approaches the Chandrasekhar limit and explodes as a Type Ia supernovae.

One way to address this issue, as well as the question of magnetism in the accreting WDs in SS, is to carry out rapid optical monitoring. The flickering^{*} seen in CVs on short (e.g., minute) time scales is presumed to come from material being accreted onto a white dwarf (Bruch 1992; Bruch & Duschl 1993; Yonehara et al. 1997; Lyubarskii 1997; Zamanov & Bruch 1998; Fritz & Bruch 1998). The detailed origin of optical flickering in CVs is not well understood, although proposed mechanisms include unstable mass transfer from the mass-donor star leading to flickering on a disk hot spot, magnetic discharges in an accretion disk, turbulence in an accretion disk, and boundary layer instabilities leading to unsteady accretion (Bruch 1992).

Flickering-type optical variability has also been reported for some supersoft sources (Crampton et al. 1997; van Teeseling et al. 1998; Meyer-Hofmeister et al. 1998). Nuclear-burning time scales and thermal time scales associated with nuclear burning on a WD are generally thought to be too long for changes associated with this burning to produce rapid optical flickering. Thus, the rapid variability in supersoft sources may instead be due to the re-processing of nuclear-burning light (which is emitted predominantly in the soft X-ray regime) into the optical by a disk rim whose height, and therefore reprocessing area/volume, changes rapidly (Meyer-Hoffmeister et al. 1998). Nuclear burning on the surface of a WD is also a major source of luminosity in some SS. Reprocessed into the optical by the surrounding nebula, it could therefore significantly affect the optical variability properties of symbiotic systems.

Symbiotics are particularly interesting for the study of rapid variability because some flicker and some do not. An early search for rapid variability in SS was conducted by Walker (1977), who observed 16 southern symbiotics from the South African Astronomical Observatory. Using a 0.5 and a 1 meter telescope, with typical observations lasting about 30 minutes, and with a time resolution of 1 - 5 seconds, he found that only the symbiotic recurrent novae (which by the nature of their thermonuclear outbursts are clearly not steadily burning fuel[†]) had rapid variability with amplitude greater than his detection limit of 1 - 2%. In 1996, a survey of 8 northern hemisphere symbiotics was performed by Dobrzycka et al. (1996). With observations up to almost 5 hours in length, they detected rapid variability in one of the

^{*} We refer to any stochastic or aperiodic brightness variations as ‘flickering’, even if the amplitude of these variations is small. CV-like stochastic variability of up to tenths of magnitudes is termed ‘large-amplitude’ or ‘strong’ flickering, whereas the smaller variations seen in the symbiotics discussed in section 5.2 will be referred to as ‘small-amplitude’ or ‘weak’ flickering.

[†] A possible exception is T Pyx (Patterson et al. 1998).

Table 1. Symbiotic Binaries in Relation to Other White Dwarf Accretors

	Cataclysmic Variables	Supersoft Sources	Symbiotics
Orbital Period:	Hours	Hours - Days	Years
Mass Transfer Mechanism:	Stable RLOF ^a	Unstable RLOF	Wind or RLOF
\dot{M}_{WD} (M_{\odot} yr ⁻¹) ^b :	10 ⁻¹⁰ – 10 ⁻⁸	10 ⁻⁸ – 10 ⁻⁶	10 ⁻⁹ – 10 ⁻⁵
Observed Number:	400-500	≈ 35	≈ 190
Magnetic Subclass:	Yes	?	Yes
Outbursts:	TNR ^a & DI ^a	Cause?	Cause?
Disk:	Yes	Yes	Some?
Steady Nuclear Burning:	No	Yes	Some
Flickering:	Yes	Some	Some

^a RLOF = Roche lobe overflow; TNR = thermonuclear runaway; DI = disk instability

^b \dot{M}_{WD} is the time-averaged accretion rate onto the white dwarf.

two recurrent novae they observed, RS Oph, plus they detected variability in two additional objects: MWC 560 and CH Cyg. They speculated about a possible inverse correlation between the hot component luminosity and presence of flickering. Our survey builds upon this previous work.

1.2 Periodic Variability from Magnetic Accretion

In CVs with a sufficiently large WD magnetic field, the accretion flow is funneled onto the WD polar caps, where the mostly radial accretion forms a stand-off accretion shock. The heated gas behind the shock produces X-ray emission, and through reprocessing at the stellar surface, optical light (Patterson 1994). The magnetospheric radius, r_{mag} , is where the magnetic pressure of the WDs dipolar field, $B \approx B_s(R/r)^3$ (where B_s is the magnetic field at the WD surface, and r is the distance from the center of the star), is comparable to the ram pressure of the accreting matter. Setting these two pressures equal gives

$$\frac{r_{\text{mag}}}{R} \approx 10 \left(\frac{R}{10^9 \text{ cm}} \right)^{5/7} \left(\frac{B_s}{10^6 \text{ G}} \right)^{4/7} \times \left(\frac{10^{-8} M_{\odot} \text{ yr}^{-1}}{\dot{M}} \right)^{2/7} \left(\frac{0.6 M_{\odot}}{M} \right)^{1/7}, \quad (1)$$

where R is the WD radius, and M is the WD mass. Thus, if a WD has $B_s \gtrsim 10^5$ G (for $\dot{M} \approx 10^{-8} M_{\odot} \text{ yr}^{-1}$), it will form a magnetosphere and, since the magnetic dipole is typically not aligned with the rotation axis, produce emission that is modulated on the WD spin period. Indeed, DQ-Her-like objects, which contain magnetized WDs accreting at rates roughly comparable to those in SS, pulsate in the optical at $\sim 10 - 100$ mmag levels (Patterson 1994). The WD spin period, P_s , is determined by the amount of angular momentum the WD has received from the accreting material, or in other words, how much it has been “spun up”. The shortest possible P_s for steady magnetic accretion is the Kepler period at the magnetosphere, $P_{\text{eq}} = 2\pi(r_{\text{mag}}^3/GM)^{1/2}$, or

$$P_{\text{eq}} \approx 12 \text{ min} \left(\frac{R}{10^9 \text{ cm}} \right)^{18/7} \left(\frac{B_s}{10^6 \text{ G}} \right)^{6/7}$$

$$\times \left(\frac{10^{-8} M_{\odot} \text{ yr}^{-1}}{\dot{M}} \right)^{3/7} \left(\frac{0.6 M_{\odot}}{M} \right)^{5/7}. \quad (2)$$

If the WD is spinning faster than P_{eq} , the disk material at the magnetospheric radius will be orbiting less rapidly than the magnetosphere is spinning, and thus will tend to slow the WD down rather than speed it up. With a minimal accretion torque $N = \dot{M}(GMR)^{1/2}$, the time for a WD in a symbiotic system to reach the equilibrium spin period, P_{eq} , is $t_{\text{spin-up}} = 2\pi I/NP_{\text{eq}} \approx 4 \times 10^5 \text{ yr}(10 \text{ min}/P_{\text{eq}})(10^{-8} M_{\odot} \text{ yr}^{-1}/\dot{M})$, where I is the moment of inertia of the white dwarf. This spin-up time is shorter than the red-giant lifetime, so the WD can reach P_{eq} if it continually receives angular momentum at this rate. Also, from equation (2) we see that minutes to tens of minutes are the interesting time scales for the search for magnetic WDs in SS. Note that these same time scales are also the important ones to examine for some WD pulsations. The nuclei of planetary nebulae have been seen to pulsate with period of tens of minutes (Ciardullo & Bond 1996), and the first pulsating WD in a CV, with periods ranging from a few to tens of minutes, was recently found by van Zyl et al. (1999).

There are several motivations for a search for magnetic WDs in SS. First of all, theories of the origin of magnetism in WDs and theories of binary stellar evolution indicate that some SS should contain WDs with strong magnetic fields (Yungelson et al. 1995; Sion et al. 1988; Angel et al. 1981). If magnetic WDs have evolved from the magnetic Ap and Bp stars, then the fraction of WDs in binaries such as symbiotics, CVs, and supersoft sources should be higher than the fraction that are magnetic in the field (which is about 2%; Anselowitz et al. 1999). The different magnetic fractions should exist because the WDs in interacting binaries come from progenitor populations that have, on average, higher masses. These progenitor populations will therefore contain a higher fraction of magnetic Ap and Bp stars than the progenitor population for field white dwarfs. In fact, 5 - 10 percent of CVs contain white dwarfs with magnetic fields $B_s \gtrsim 10^5$ G (Wickramasinghe & Ferrario 2000). This high magnetic fraction could, however, be due to selection effects,

as some CVs are found by their optical or X-ray pulsations. Magnetic symbiotics have a different set of selection effects, and therefore provide an interesting testing ground for these theories.

Secondly, the flickering and other properties of several symbiotics (CH Cyg and MWC 560) have led Mikołajewski et al. (1990ab), Mikołajewski & Mikołajewska (1988), Tomov et al. (1992), and Michalitsianos et al. (1993) to propose that these systems contain magnetic propellers. The detection of a magnetic WD in a SS by another means, such as discovery of a coherent oscillation, would allow a test of these propeller models if the new magnetic system were to experience a change in accretion rate.

Finally, the brightness oscillation associated with the spin of a magnetic, accreting WD in a symbiotic can be a useful diagnostic tool for these complex systems, as has already been seen in the case of Z And (Sokoloski & Bildsten 1999). Also, such systems provide an opportunity to study magnetically controlled accretion in an environment that is quite different from CVs.

1.3 Our Search for Rapid Variability

The study of rapid variability from SS can help elucidate the relationship between SS and other accreting WD systems by providing direct information about the nature of the accretion region in SS, as well as the surrounding nebula. Building upon previous work by other authors (discussed in §1.1), we observed 35 northern symbiotics between 1997 January and 1999 July. Five of the survey objects are previously-known flickerers (*o* Ceti = Mira AB, MWC 560, CH Cyg, and the recurrent novae T CrB and RS Oph). In this paper, we present our observations for 29 of the survey objects that have no previous detections of rapid variability. Seven of these 29 objects were included in the other searches for rapid variability mentioned above. Our observations of the well-known flickerers and the serendipitous discoveries, including a possible new short-period δ Scuti star, are discussed in separate papers (Sokoloski et al. 2001a,b). Our results for Z And, where we discovered the first stable, coherent oscillation ever seen in a symbiotic, are also presented in a separate paper (Sokoloski & Bildsten 1999). We describe our observations and the properties of the survey objects in §2, and the production of light curves in §3. The timing analysis and a discussion of sources of error are presented in §4. We display and discuss the results from both the non-flickering systems and the marginal flickering candidates in §5. Finally, in §6 we consider the implications of our results for the properties of the nebulae, accretion structures, and sources of power in symbiotic stars.

2 THE SURVEY

2.1 Observations

All of the observations presented here were performed using the 1-meter Nickel telescope at UCO/Lick Observatory on Mt. Hamilton, near San Jose. In order to search for rapid variability, we used time-resolved differential CCD photometry. This procedure involved the repeated measurement of the program star flux relative to an ensemble average of the

fluxes of other stars in the field (the “comparison stars”). Each observation consisted of a series of exposures with either the unthinned, 2048×2048 Loral CCD (“CCD 2”; 15μ pixels), or on several occasions (fewer than 10% of the total number of observations) the thinned, 1024×1024 SITE CCD (“CCD 5”; 24μ pixels). The field of view for CCD 2 is $6.3' \times 6.3'$, and the field of view for CCD 5 is $5.0' \times 5.0'$. Exposure times ranged from 4 to 100 seconds, with a dead time between exposures of roughly 15 to 28 seconds for chip read-out and pre-processing, depending upon the number of rows read out. A Johnson-Cousins *B* filter was used for most observations. This filter was selected to reduce the amount of light detected from the red giant, while still allowing for a large enough detected flux to produce high signal-to-noise ratio (S/N) measurements in about one minute. For several extremely bright objects, a liquid CuSO_4 (+1mm UG2) *U*-band filter was used, and if multiple observations were done for a single object, a *U*-band observation was sometimes included. Table 2 is the complete log of the observations described in this paper. A typical observation lasted 3 to 4 hours, and so 1 to 3 observations were performed per night.

The exposure times were chosen to maximize the resulting S/N, while not saturating the program star or any comparison stars, and while keeping the time between individual exposures to less than 2 minutes. Longer integrations would have reduced our sensitivity to oscillations with periods in the interesting range of a few to tens of minutes, and to the most rapid flickering. We also generally avoided exposures of just a few seconds, since for short exposures the comparatively long read-out time would have made the duty cycle low, and the observations rather inefficient.

In order to obtain evenly spaced exposures and thus produce data sets compatible with standard fast Fourier transform (FFT) routines, we usually employed a timing system developed especially for this project by Will Deitch. Therefore, for most of the observations, the time between exposure starts was constant to very high precision. This timing system was not available when our earliest observations were done. For some of these early observations, the time between exposures varied by 1 - 2 seconds, or about 5 - 10%[‡].

2.2 Differential CCD Photometry

Differential CCD photometry can yield useful data even when the weather conditions are not ideal. Assuming the point-spread function is the same for each star on the chip, and that clouds reduce the count rate for each object by the same fraction, the ratio of fluxes extracted from the same aperture for constant brightness stars should remain constant despite variable clouds and/or seeing changes. Two

[‡] The early version of our timing system introduced some timing error that affected our sensitivity to periodic oscillations. Since we arrived at our pulse amplitude upper limits by repeatedly injecting oscillations into our real data using the same sampling as the real light curve, however, the upper limits derived in this way remain valid. Comparisons between simulations with even sampling and slightly uneven sampling, as we had in our early data, indicate that the sensitivity to periodic oscillations is reduced by a few percent.

Table 2. Observation Log for Lick Symbiotic Survey

Binary Name	Date, U.T. (m/d/yr)	Obs. Start (<i>MJD</i>)	Obs. Length (hr)	$t_{exp}/$ Δt^a (s)	Number of Points ^b	Filter	Detector (CCD 2 or 5)
EG And	1/17/97	50465.150	0.9	90.0/109.452	31	<i>U</i>	2
	7/9/97	50638.450	1.2	45.0/67.0	63	<i>U</i>	2
	7/11/97	50640.437	1.6	4.0/28.0	208	<i>B</i>	2
	9/16/98	51072.296	5.6	90.0/112.855	159	<i>U</i>	5
AX Per	1/23/98	50836.127	3.9	90.0/118.0	96	<i>B</i>	2
	9/15/98	51071.354	4.5	40.0/66.226	225	<i>B</i>	5
V471 Per	8/22/98	51047.430	2.3	80.0/106.221	76	<i>B</i>	5
S 32	3/13/97	50520.082 ^c	1.3 ^b	70.0/≈ 94.3 ^b	46	<i>B</i>	2
	9/14/98	51070.444	2.2	70.0/96.191	73	<i>B</i>	5
UV Aur	11/2/97	50754.447	3.2	30.0/53.0	212	<i>B</i>	2
BX Mon	1/18/97	50466.288	0.3	90.0/115.444	10	<i>B</i>	2
	2/16/97	50495.174	5.1	60.0/85.261	208	<i>B</i>	2
	3/12/97	50519.232	3.1	100.0/125.478	87	<i>U</i>	2
	4/7/97	50545.165	1.0	60.0/85.122	42	<i>B</i>	2
	11/1/97	50753.460	2.6	80.0/102.0	88	<i>B</i>	2
TX CVn	3/13/97	50520.180 ^b	3.2 ^b	60.0/≈ 87.8 ^b	105	<i>B</i>	2
RW Hya	2/18/97	50497.439	2.1	30.0/55.478	132	<i>B</i>	2
BD-21.3873	5/14/97	50582.232	2.0	100.0/114.841	61	<i>B</i>	2
	5/31/98	50964.263	1.8	70.0/90.0	68	<i>B</i>	2
AG Dra	6/7/97	50606.294	3.3	22.0/47.212	255	<i>B</i>	2
	7/23/98	51017.203	4.7	55.0/82.0	200	<i>B</i>	2
HD 154791	8/4/97	50664.178	2.0	7.0/34.0	514	<i>B</i>	2
Hen 1341	6/28/98	50992.222	2.3	60.0/94.0	88	<i>B</i>	2
AS 289	5/31/98	50964.373	2.6	90.0/111.0	75	<i>B</i>	2
YY Her	5/14/97	50582.339	3.9	50.0/75.571	168	<i>B</i>	2
AS 296	8/21/98	51046.193	3.1	90.0/115.010	94	<i>B</i>	5
S 149	5/15/97	50583.408	2.2	60.0/85.404	94	<i>B</i>	2
	8/20/98	51045.176	4.6	50.0/76.995	205	<i>B</i>	2
V443 Her	4/7/97	50545.429	2.8	60.0/78.433	125	<i>B</i>	2
FN Sgr	6/30/98	50994.347	2.8	20.0/48.0	210	<i>B</i>	2
CM Aql	9/16/98	51072.153	2.9	100.0/120.209	86	<i>B</i>	5
V919 Sgr	8/22/98	51047.206	2.5	90.0/116.263	77	<i>B</i>	5
BF Cyg	4/6/97	50544.429	2.5	50.0/75.317	115	<i>B</i>	2
	7/11/97	50640.212	4.1	50.0/78.0	185	<i>B</i>	2
	7/1/98	50995.260	5.6	80.0/108.0	176	<i>B</i>	2
CI Cyg	6/8/97	20607.256	3.1	25.0/43.557	252	<i>B</i>	2
	9/15/98	51071.151	4.4	100.0/126.2	98	<i>U</i>	5
AS 360	6/29/98	50993.214	2.3	50.0/78.0	104	<i>B</i>	2
PU Vul	6/15/97	50614.442	1.4	40.0/58.643	77	<i>U</i>	2
He2-467	8/22/98	51047.326	2.1	90.0/116.154	64	<i>B</i>	5
S 180	7/23/98	51017.434	1.5	100.0/127.0	38	<i>B</i>	2
S 190	8/21/98	51046.344	3.4	50.0/65.995	186	<i>B</i>	5
AG Peg	9/17/98	51073.148	4.5	20.0/47.0	280,170	<i>B</i>	5
R Aqr	9/14/98	51070.261	3.9	30.0/51.451	265	<i>B</i>	5

^a t_{exp} is the exposure time, and Δt is the average time between exposure starts.

^b The number of data points used in the analysis is equal to the number of images taken minus those affected by cosmic rays, extremely poor weather, or other problems. If two values are given, the first is for the light curve, and the second is for the power spectrum.

^c The times between data points are only approximate on 1997 March 13 due to a clock problem.

examples of the usefulness and capabilities of differential photometry are shown in Figures 1 and 2. In Figure 1, raw light curves are shown for the symbiotic V443 Her, another star in the same field of view, and the differential light curve. Even though each of the raw light curves has dips due to

clouds or changes in seeing, the differential light curve is flat to within the error bars. Using differential photometry, we can thus place an upper limit on the intrinsic variability of V443 Her. In Figure 2, raw light curves for the symbiotic star T CrB and another star in its field are shown, as well

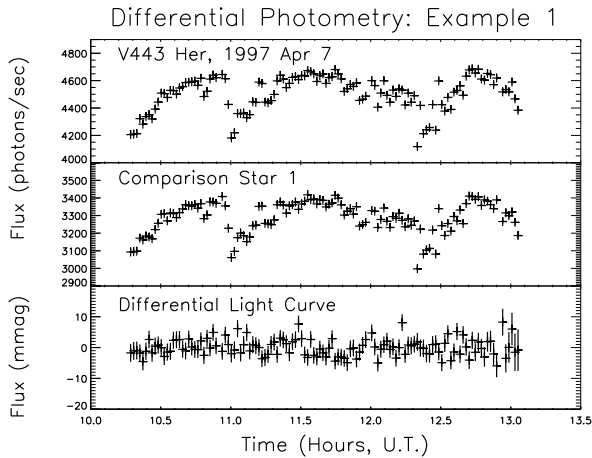


Figure 1. Example of the capabilities of differential photometry. In the top panel, the raw light curve for V443 Her from 1997 April 7 (U.T.) is shown. The raw light curve for a second star in the field is shown in the middle panel. In both cases, dips due to clouds or other atmospheric changes are evident. In the bottom panel, the differential light curve formed from the ratio of V443 Her and an ensemble average of 4 comparison stars is shown. The atmospheric variability is completely removed.

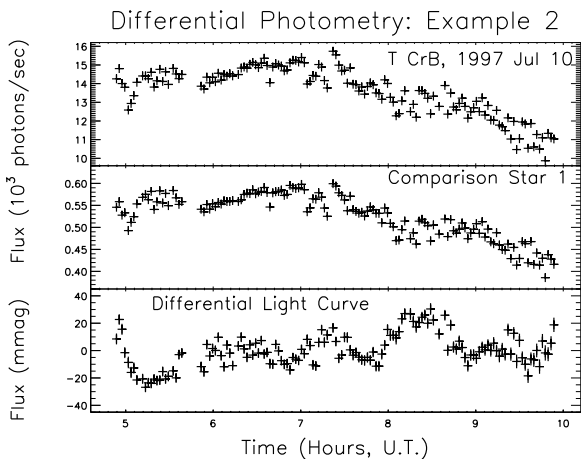


Figure 2. A second example of the capabilities of differential photometry. For this observation of T CrB, we were able to remove the atmospheric effects and see the variability intrinsic to the source. The differential light curve was created with an ensemble average of 4 comparison stars.

as the differential light curve. Again, the raw light curves show variability due to clouds, seeing changes, and variable air mass. But this time the ratio shows that T CrB is in fact intrinsically variable.

2.3 Sensitivity to an Oscillatory Signal

Before describing our techniques in more detail, we give an estimate of our sensitivity. A typical symbiotic star has a $B \approx 12$. The photon count rate for an object of magnitude m is given by

$$N_c = N_0 10^{-m/2.5} \times \text{area} \times \text{bandwidth} \times QE, \quad (3)$$

where $N_0 \approx 1400 \text{ cm}^{-2} \text{ s}^{-1} \text{ \AA}^{-1}$ (the flux density for a $B = 0$ object), “area” is the mirror collecting area, “bandwidth” is the effective bandwidth obtained by integrating over the transmission of the filter and the atmosphere, and QE is the quantum efficiency of the CCD. Plugging in an area of 7850 cm^2 (not taking into account the secondary mirror blockage), an effective bandwidth of 380 \AA (for an airmass of 1.5 and using extinction tables from Hayes & Latham 1975), and a quantum efficiency of 0.15 (rough estimate for Lick’s CCD 2), we find $N_c \approx 9900 \text{ photons/sec}$ for $B = 12$. If uncertainties are set purely by photon counting statistics of the source (e.g., if all comparison stars are much brighter than the program star, the background is low, and systematic uncertainties are negligible), then the S/N for detection of a pulsed signal is given by

$$\frac{\text{Signal}}{\text{Noise}} = \frac{(1/4)pN_c t}{\sqrt{N_c t}}, \quad (4)$$

where p is the pulse fraction, and t is the total integration time. The factor of $1/4$ in the numerator of equation (4) comes from the fact that we want to divide the signal counts into at least 4 phase bins. If we demand a S/N of 5 (in each phase bin), and we assume 3 hours of total integration time, then we are sensitive to pulse fractions of the order

$$p = 0.002 \left(\frac{N_c}{9900 \text{ s}^{-1}} \right)^{-1/2} \left(\frac{t}{3 \text{ hr}} \right)^{-1/2}, \quad (5)$$

for a $B = 12$ star. This rough estimate is comparable to the result of the more careful calculation given in equation (26). In practice, we cannot quite reach this level, as explained in the detailed discussion in §3.

2.4 Source Selection

Table 3 lists the binaries included in our survey. They were taken from the lists of Kenyon (1986) and Downes & Keyes (1988), and were selected primarily because of their observational suitability for differential photometry timing analysis from Lick Observatory. In order to detect mmag level variability, we required roughly 10^5 stellar counts per integration. Since we wanted to probe minute-long time scales, the program star had to provide at least $\sim 800 \text{ c/s}$ within the extraction region. This count rate could generally be achieved for stars brighter than $B \approx 14$ mag with CCD 2, and for slightly fainter objects with CCD 5 (if the comparison stars were significantly brighter and therefore did not add much uncertainty). Note, however, that if there are only a few faint comparison stars (fainter than the program star at B), then these stars and not the program star set the variability-amplitude detection limit. Since typical values of $B - V$ for symbiotics lie between 0 and 1 (see Table 3), and V magnitudes were more readily available, in practice we selected objects with published V magnitudes of less than 14.

Table 3. Properties of the Symbiotics Surveyed

Name	RA(2000) (h m s)	Dec(2000) (° ' ")	IR Type	Outburst Type ^a	Hot Component ^b	L_{hot} (L_{\odot})	P_{orb} (d)	Distance (kpc)	V^c (mag)	B^c (mag)	Refs. ^d
EG And	00 44 37.2	+40 40 46	S			~ 10	482.6	0.30 - 0.35	7.5,7.2	8.8	1,3,4,5,8
AX Per	01 36 16.9	+54 15 35	S	C	MS	~ 700	680.8	2 - 3	12	10.8	1,2,3,4,5,8
V471 Per	01 58 49.7	+52 53 48	D'						13.2,13.1	14.1	1,5
Mira	02 19 20.7	-02 58 28			WD	1 - 10			3.0	4.5	2,5
S 32	04 37 45.3	-01 19 09							13.5		6
UV Aur	05 21 49.0	+32 30 44	S						7.9,9.6	11.0	1,5
BX Mon	07 25 23.9	-03 35 59	S		WD	100 - 1000	1401		12,9.5	9.5	1,2,5,8
MWC 560	07 25 51.2	-07 44 04			WD	100 - 1000	1930		9.7	10.0	2,5,8
TX CVn	12 44 42.2	+36 45 49	S	C			199		9.3,9.8	10.4	1,5,8,7
RW Hya	13 34 18.2	-25 22 49	S		WD	350	370.2	0.6 - 1.3	10,8.9	10.2	1,2,3,4,5,8
BD-21.3873	14 16 34.3	-21 45 51	S				281.6		10.2		1,5,8
T CrB	15 59 30.2	+25 55 12	S	RN		5 - 40	227.57		10.0,10.2	11.5	1,2,5,8
AG Dra	16 01 41.0	+66 48 09	S	C	WD	1000 - 10000,10-20	554	0.4 - 0.7	11.2,9.8	11.3	1,2,3,4,5,8
HD 154791	17 06 34.5	+23 58 18			NS				7.6	9.2	5
Hen 1341	17 08 36.7	-17 26 29	S					2.4	12.0		1,3
RS Oph	17 50 13.2	-06 42 27	S	RN	WD	~ 100	455.7	0.6	11.5		1,2,4,8
AS 289	18 12 22.2	-11 40 07	S					1.0		10.5	1,4
YY Her	18 14 34.1	+20 59 18	S	C		~ 1000	590	3.8 - 5.1	12	11.7	1,3,5,8
AS 296	18 15 06.4	-00 18 59	S	SN				1.8	10.5	13.5	1,4,5
S 149	18 18 56.2	+27 26 10							13.5		6
V443 Her	18 22 07.7	+23 27 20	S		WD	~ 1000	594	1.9 - 2.7	11.5	12.4	1,2,3,4,5,8
FN Sgr	18 53 54.4	-18 59 42	S	C			567.2	5.0	11	9.0	1,4,5,8
CM Aql	19 03 35.1	-03 03 14	S	C					15	13	1,5,8
V919 Sgr	19 03 45.1	-16 59 54	S					2.1	12.5,11.8	12.5	1,4,5
BF Cyg	19 23 53.4	+29 40 28	S	C	WD	3000,5000	756.8	2.6 - 5.0	12,10.3	10.6	1,2,3,5,8
CH Cyg	19 24 33.1	+50 14 29	S		WD	1 - 10	5700?	0.22 - 0.4	7,8.8	10.2	1,2,3,4,5,8
AS 360	19 45 49.3	+18 36 45	S					10.0	11.0	11.0	1,4,5
CI Cyg	19 50 12.2	+35 41 03	S	C	MS	3000 - 5000,560	855.3	1.2 - 2.1	11.1	11.9	1,2,3,4,5,8
PU Vul	20 21 13.3	+21 34 18	S	SN	WD	~ 1000	4900	6.0	9,8.5	11.7	1,2,4,5,8
He2-467	20 35 57.3	+20 11 33	S						13		1
S 180	20 39 20.6	-05 16 58							13.5		5,6
S 190	21 41 45.0	+02 43 53							10.3,10.5	11.1	5,6
AG Peg	21 51 02.2	+12 37 31	S	SN	WD	~ 1000	816.5	0.60 - 0.72	9.4,8.7	9.8	1,2,3,5,8
Z And	23 33 40.0	+48 49 06	S	C	WD	500 - 2000	758.8	0.98 - 1.6	10.5	11.9	1,2,3,5,8
R Aqr	23 43 49.5	-15 17 02	S/D ^c		WD	1 - 100	16000		5.8,7.7	8.8	1,2,5,9

^aC = classical symbiotic outburst = Z-And-type outburst; RN = recurrent nova; SN = symbiotic nova = symbiotic slow nova.

^bObjects listed as “hot stellar sources” (HSS) by Dobrzycka et al. (1996) are listed here as WDs. HD 154791 is the one neutron star system.

^cIf more than one value is given, the different values are from different authors. Note that symbiotics are variable, so the V magnitudes given may not reflect current source brightnesses. These magnitudes are, however, typical values for most objects.

^d(1) Kenyon 1986, (2) Dobrzycka et al. 1996, (3) Mürset et al. 1991, (4) Seaquist & Taylor 1990, (5) SIMBAD, (6) Downes & Keyes 1988, (7) Kenyon & Garcia 1989, (8) Belczyński et al. 2000, (9) Willson et al. 1981, and references therein for all.

For the survey, slow novae still in outburst were generally avoided, since the expanded envelopes in these systems would hide any rapidly variable processes near the surface of the WD. However, a few slow-novae-like systems and slow novae well after decline from maximum were observed (PU Vul, AG Peg, and AS 296). Finally, since Lick Observatory is at 37° latitude, we could only produce reasonable light curves for symbiotics with $\delta \gtrsim -25^\circ$. In the end, we observed all of the objects from Kenyon (1986) and Downes & Keyes (1988) that were not slow novae, and that have $V < 14$ mag and $\delta > -20$, except one. In addition, we observed 2 objects that were slightly more southern (RW Hya and BD-21.3873), one slightly fainter object (CM Aql), the symbiotic-like systems Mira AB (*o* Ceti) and MWC 560, and the neutron-star symbiotic HD 154791, for a total of 35 objects. Most of the symbiotics we observed presumably contain WD accretors (Mürset et al. 1991), although the 2 strongest candidate main-sequence systems (CI Cyg and AX Per; see Kenyon et al. 1991, Mikołajewska & Kenyon 1992a, and references therein) are also included in our sample. All of the symbiotics in the sample are IR S-types, except for one D'-type system[§] (V471 Per). Some properties of the survey objects are listed in Table 3. The previously-known flickerers and Z And are included for comparison, even though we present our observations of these systems elsewhere.

3 DATA REDUCTION

A typical observation, or series of exposures, produced between 50 and 250 images, and the complete survey consisted of over 80 such observations. Roughly half of these observations were of the previously-known flickering systems, and the other half are presented here. The data reduction and analysis was done in IDL, and it included the use of software based upon standard IRAF routines. For each observation, the data were reduced using the standard techniques (e.g. Gilliland 1992).

3.1 Estimation of Uncertainties

Before describing the aperture photometry and generation of light curves, we discuss our method for estimating the uncertainties in the CCD photometry. An understanding of the uncertainties is crucial for identification of low-level variability intrinsic to the source, especially low-level flickering-type variability. We found the formal uncertainties for each star in each image from the CCD equation (equation 6) and Young's expression for expected atmospheric scintillation. The uncertainty in CCD aperture photometry is given by

$$\sigma_{CCD}^2 = c + n_{bins} \left(1 + \frac{n_{bins}}{n_{sky}}\right) (N_S + N_R^2 + N_D) \quad (6)$$

(Howell 1992), where c is the number of integrated stellar source counts in electrons (or photons), n_{bins} is the area of the software aperture in bins, n_{sky} is the area of the region

[§] The notation D' is sometimes used to indicate a D-type symbiotic with a yellow absorption line spectrum, as opposed to a Mira-containing D-type with deep CO and H₂O absorption bands. (S. Kenyon, private communication).

used for background estimation in bins, N_S is the sky (background) counts (electrons/bin), N_R is the read noise (in rms electrons/bin), N_D is the dark current (electrons/bin). We refer to bins instead of pixels, because we always used CCD 2 with 4×4 pixel binning and CCD 5 with 2×2 pixel binning. Not included in equation (6) is digitization error, which is less than the value of the gain (typically $6.8 e^-/ADU$ and $7.7 e^-/ADU$ for our two CCDs), and therefore always negligible for us.

For our observations, N_S generally ranged from 50 to 500, read noise squared had the values $N_R^2 \approx 100 - 150$, and the dark current was $N_D < 1(t_{int}/100 \text{ s})$. Therefore, we can drop the dark-current term and rewrite the uncertainty as

$$\sigma_{CCD}^2 \approx c + n_{bins} (N_S + N_R^2) + \frac{n_{bins}^2}{n_{sky}} (N_S + N_R^2). \quad (7)$$

The number of stellar counts, c , was typically a few times 10^4 to 10^6 . The second term, $n_{bins} (N_S + N_R^2)$, which arises from Poisson fluctuations of the background and readnoise within the aperture, was approximately 10^4 for low-background periods, but could approach 10^5 when a bright moon and clouds were present. The average background count rate for an observation was primarily a function of the phase of the moon, whether or not there were low clouds blocking the light from San Jose, and the cloud-cover overhead. The third term arises from the Poisson uncertainty in the estimation of the background level, and was a factor of $n_{bins}/n_{sky} \approx 0.1$ smaller than the second term. In the data analysis, the formal uncertainties were calculated by replacing the expression $N_S + N_R^2$ in equation (7) with the measured variance from the sky annulus. This was a conservative approximation, as the measured variance should be greater than or equal to $N_S + N_R^2$.

In addition to Poisson uncertainties, there was also an inescapable contribution to source variability from atmospheric scintillation. Scintillation refers to the brightness variations of a star viewed through a finite aperture pupil due to temperature-related fluctuations in the refractive index of the atmosphere. As the spatial refractive-index fluctuations in the turbulent atmosphere move between the telescope and the star at the wind speed, the wavefront is perturbed, and the amount of starlight received by the telescope will vary. According to Young's formulation (Young 1967) of Reiger's theory of scintillation (Reiger 1963),

$$s_{scint} = \frac{c_{rms}}{\bar{c}} = S_0 d^{-2/3} X^{3/2} e^{-h/h_0} \Delta f^{1/2}, \quad (8)$$

where s_{scint} is the fractional rms variation due to scintillation[¶], c_{rms} is the rms variation in the source counts, \bar{c} is the mean value of the number of source counts, c , from a series of measurements, S_0 is a constant that Young (1967) determined empirically to be 0.09, d is the mirror diameter in cm, X is the air mass, h is the observatory altitude in meters, $h_0 = 8000$ m, and Δf is the frequency bandpass of

[¶] We will often express fractional rms variation in units of mmag. For a change in flux ΔF that is small compared to the average flux F , we have $\Delta m = 2.5 \log((F + \Delta F)/F) = (2.5/\ln 10) \ln(1 + \Delta F/F) \approx 1.086(\Delta F/F)$, where Δm is the magnitude change corresponding to ΔF . Therefore, a 0.1% flux variation is approximately equal to a magnitude change of 1 mmag.

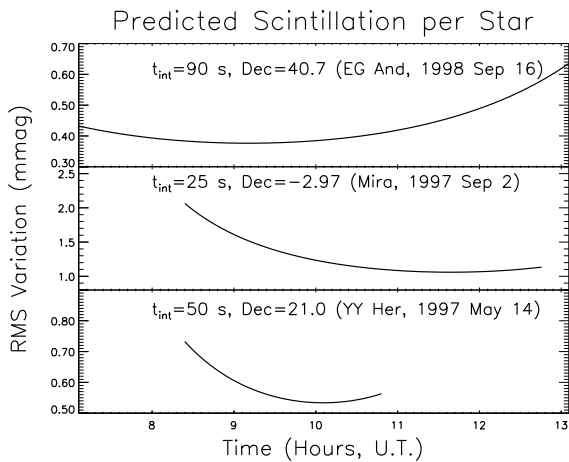


Figure 3. RMS variation due to scintillation per star for three typical observations. The amplitude of the scintillation variability is a function of integration time and airmass.

time-series sampling rate in Hz^{||} (i.e. $\Delta f = 1.0/t_{int}$, where t_{int} is the integration time for each exposure in seconds). The expression for the total formal photometric error for each star in a field is thus

$$\sigma_m^2 = \sigma_{CCD,m}^2 + s_{scint}^2 c_m^2, \quad (9)$$

where $\sigma_{CCD,m}$ is σ_{CCD} from equation (6) for star m with c_m source counts.

For the Nickel telescope at Lick Observatory, where $d = 100$ cm and $h = 1280$ m, and scaling to typical values of air mass and integration time, we find

$$s_{scint} = 0.84 \text{ mmag} \left(\frac{S_0}{0.09} \right) \left(\frac{d}{100 \text{ cm}} \right)^{-2/3} \left(\frac{X}{1.5} \right)^{3/2} \times e^{-h/1280 \text{ m}} \left(\frac{t_{int}}{60 \text{ s}} \right)^{-1/2}. \quad (10)$$

Assuming $S_0 = 0.09$ is applicable to our observations (this is a conservative assumption, since whereas Young (1967) measured this value for McDonald Observatory, Gilliland & Brown (1992) inferred a value of 0.07 for Kitt Peak National Observatory and speculated that even this value might be an upper limit), we then find that even for the lowest airmass of 1.0, we still have 0.5 mmag contribution to the rms variation from scintillation for $t_{int} = 60$ s. The contribution climbs to 1.8 mmag for $X = 2.5$ (and $t_{int} = 60$ s), which is comparable to the standard deviation from Poisson statistics for our typical count rates. Figure 3 shows the rms variation due to scintillation for several typical observations. Note that variability due to scintillation is independent of the software extraction aperture size.

^{||} The frequency bandpass scaling of s_{scint} arises from the fact that the power spectrum of scintillation is flat (Reiger 1963; Young 1967), up to a high frequency cutoff. Since the variance is proportional to the integral of the power, $s^2 \propto \int_{f_1}^{f_2} P(f) df \propto f_2 - f_1$, where $f_2 \propto 1/t_{int}$ is the Nyquist frequency and $f_1 \rightarrow 0$, the rms deviation s_{scint} is proportional to $t_{int}^{-1/2} \propto \Delta f^{1/2}$.

3.2 Aperture Photometry and Construction of Light Curves

For the program star and as many comparison stars as possible (usually 2 to 6), the counts were extracted from circular apertures with radii that typically ranged from 4.0 to 8.0 bins for CCD 2 and 5.0 to 9.5 bins for CCD 5 (3 to 6 arcsec in both cases). The background was estimated from an annulus surrounding the star of interest. Very faint comparison stars were not used, because for faint objects, the increased number of data points that became unusable due to cosmic ray contamination outweighed the small improvement in the S/N of the final light curve. Stars with blended images were also not used as comparisons. We elected to use simple aperture photometry instead of point-spread function (PSF) fitting for several reasons. First, most of our fields did not contain many stars, and the PSFs for these stars were not well sampled due to our coarse binning. Second, the PSFs changed significantly as a function of time, so that a reliable PSF would have been difficult to obtain.

For each image in a sequence of N images used to produce a light curve, the ratio of the program star counts to a weighted sum of comparison star counts was found:

$$x(i) = A \frac{c_p(i)}{\sum_{m=1}^K w_m c_m(i)}, \quad i = 0, \dots, N-1 \quad (11)$$

where $x(i)$ is the count ratio for the i^{th} image, $c_p(i)$ is the background subtracted source counts for the program star in the i^{th} image, $c_m(i)$ is the background subtracted source counts for the m^{th} comparison star in the i^{th} image, w_m is the weight for the m^{th} comparison star (same for every image, i), K is the number of comparison stars used, and A is a normalization factor,

$$A^{-1} = \frac{1}{N} \sum_{j=0}^{N-1} \frac{c_p(j)}{\sum_{n=1}^K w_n c_n(j)}. \quad (12)$$

The weights are given by

$$w_m = \frac{\overline{c_m}}{\overline{\sigma_m^2}} = \frac{\sum_{i=0}^{N-1} c_m(i)}{\sum_{i=0}^{N-1} \sigma_m^2(i)}, \quad (13)$$

where σ_m is the formal uncertainty on c_m , the source counts for star m , from equation (9), and $\overline{c_m}$ and $\overline{\sigma_m^2}$ are the averages of c_m and σ_m^2 over all N images. This form of the weights can be derived by minimizing the uncertainty in the count ratio $x(i)$ (given in equation (14)). Note that the weights go to 1 in the Poisson limit of $\sigma_m^2 = c_m$. This weighting scheme is the same as that used by Gilliland & Brown (1988), except that no position or color information is included. The series of x values has been normalized to unity, so a variation of 0.001 in x corresponds closely to 1 mmag. We refer to the series of x values as the light curve, and individual x values as data points. The formal uncertainty for each data point can be expressed as a function of the uncertainties for the individual program and comparison stars:

$$\sigma_x^2(i) \approx \left(\frac{\sigma_x(i)}{x(i)} \right)^2 = \left(\frac{\sigma_p(i)}{c_p(i)} \right)^2 + \frac{\sum_{m=1}^K (w_m \sigma_m(i))^2}{\left[\sum_{n=1}^K w_n c_n(i) \right]^2}. \quad (14)$$

The variance is approximately equal to the fractional variance in the expression above because, for the data presented here, the $x(i)$ are all very close to unity.

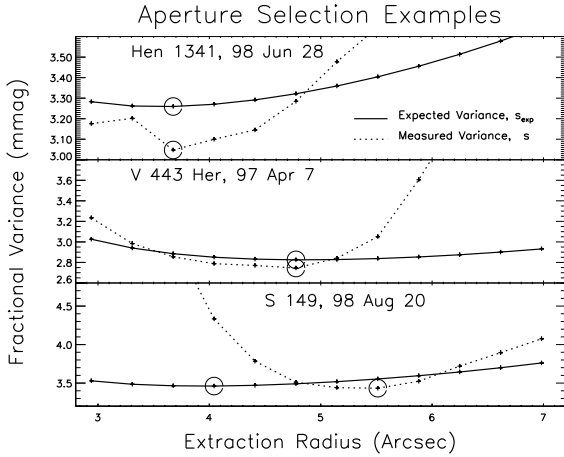


Figure 4. Three examples of the expected and measured rms variation as a function of the photometry aperture. In the first two cases, the aperture which produced the lowest expected variance also gave the lowest measured variance. The aperture used for most observations was that which produced the lowest expected variance, even if that aperture did not produce the lowest measured variance. The third panel shows an example of a case where systematic errors were determined to be present at small apertures, so a larger aperture was used. In each of these examples, 4 comparison stars were used in the construction of the light curves.

In constructing the final light curve, the aperture selected was generally the one that maximized the S/N, or in other words, minimized the expected variance s_{exp}^2 , where s_{exp}^2 is a weighted average of the σ_x^2 over all the points in a light curve,

$$s_{exp}^2 = \frac{\sum_{i=0}^{N-1} \left(\frac{1}{\sigma_x^2(i)} \sigma_x^2(i) \right)}{\sum_{i=0}^{N-1} \frac{1}{\sigma_x^2(i)}} = \frac{N}{\sum_{i=0}^{N-1} \frac{1}{\sigma_x^2(i)}}. \quad (15)$$

On the few occasions when the aperture which produced the best formal S/N was very small (radius less than about 4 bins, or $3''$ for CCD 2), a slightly larger aperture was actually used to avoid problems with pixelization noise or other systematic uncertainties if these systematic errors were seen to be present in the comparison stars at small extraction radii. Pixelization noise was only a problem for small apertures (see section §4.3). A single aperture was used in extracting counts for the program and all comparison stars throughout an entire light curve. The use of different apertures for different parts of the light curve would improve the formal S/N, as the background generally changed throughout an observation. However, we chose not to do this, as it would introduce a new source of error because the PSFs are not quite the same for the different stars in the field. For observations with a low background count rate, using a larger aperture increased the source counts extracted without significantly increasing counts from the background, and therefore improved the S/N. For observations with a high background rate, on the other hand, smaller apertures reduced the uncertainty introduced by the background light and therefore produced higher S/N light curves. A few typical plots of s_{exp} as a function of aperture, as well as the measured rms variation, are shown in Figure 4.

Data points contaminated by radiation events (“cosmic rays”) were omitted, as were points with extremely high background, or taken during exceptionally poor weather conditions. Data points contaminated by cosmic rays were identified in two ways. First, the residuals from Gaussian fitting were compared for the various stars in a field. This method worked well for cosmic rays in the wings of a PSF, but less well for cosmic rays that hit near the center of the PSF. Next, light curves were formed for all possible pairs of comparison stars in a field. If any point in these light curves was suspiciously high or low (by greater than at least 5σ , although usually much more), that point was not used in the creation of the final ensemble average. Occasionally, individual extreme high points were due to a cosmic ray hit near the program star itself, and these points were also removed. We were much more conservative, however, about removing points in which the program star was the one thought to be contaminated. In general, only about 5 to 10 points per light curve were rejected because of cosmic ray contamination. This number is consistent with the expected rate of cosmic ray hits, given the measured distribution of cosmic rays from dark images. We measured the rate of cosmic ray hits to be $1.25 \times 10^{-6} \text{ s}^{-1} \text{ bin}^{-1}$ for CCD 2. The number of contaminated data points per observation, n_{crs} , is then expected to be

$$n_{crs} \approx 5 \left(\frac{K+1}{5} \right) \left(\frac{N}{120} \right) \left(\frac{6}{b} \right)^2 \left(\frac{t_{int}}{60 \text{ s}} \right), \quad (16)$$

where K is the number of comparison stars, N is the number of data points, b is the extraction radius in bins, and t_{int} is the integration time (note that radiation events can also occur during read-out). The distribution of total counts in a cosmic-ray event, measured from two 30-minute dark images, is plotted in Figure 5. The most typical event size was approximately $200 \text{ ADU} \approx 1400 e^-$. Since a typical number of source counts was on the order of 10^5 , an unidentified cosmic ray within the stellar aperture could therefore artificially increase the source flux by roughly 1%.

Finally, the resulting light curve was fit with a 2nd or 3rd-order polynomial, depending upon the length of the observation, to remove any slow variations due to changing air mass. These variations could exist, despite using differential photometry, when the program star and comparison stars had significantly different colors.

4 TIMING ANALYSIS

The survey light curves were analyzed in several ways. First, the measured rms variation was compared to that expected from the CCD equation and scintillation. Next, power spectra were computed to search for periodic signals, and Monte Carlo simulations performed to determine our detection limits for sinusoidal variations in each light curve.

4.1 Aperiodic Variability

The crux of our search for aperiodic variability, or flickering, was comparing the measured rms variation for each light curve (denoted s) to the rms variation expected from the known errors, denoted s_{exp} , defined in equation (15). The measured rms variation is obtained from the data using the

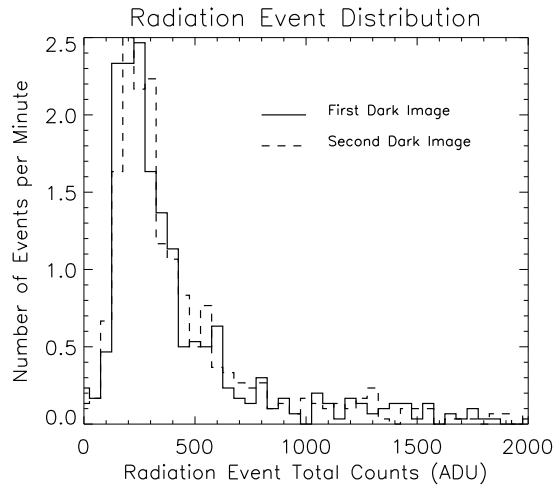


Figure 5. Energy distribution of cosmic rays, from two 30-minute dark images taken with CCD 2.

general expression for the variance when the errors on each data point are different (Bevington 1969, p. 185),

$$s^2 = \frac{N}{N-1} \frac{\sum_{i=0}^{N-1} \left(\frac{x_i - \bar{x}}{\sigma_i}\right)^2}{\sum_{j=0}^{N-1} \frac{1}{\sigma_j^2}}. \quad (17)$$

Note that comparing the two quantities s and s_{exp} is actually the same as calculating χ^2 for the hypothesis of a constant flux (Bevington 1969, p. 188). If s and s_{exp} are comparable (i.e., $s/s_{exp} \approx 1$), the fit of the data to a constant flux model is good, but if s/s_{exp} is significantly greater than 1, the fit is bad and the source is possibly variable. Plotted in Figure 6 are examples of three different types of light curves. In the top panel (UV Aur), $s/s_{exp} \approx 1$, and we find a variability upper limit of $s = 2.7$ mmag. Most light curves in our survey fall into this category, and a list of the variability upper limits is given in Table 4. In the middle panel, we present the other extreme — a light curve of the well-known flickerer CH Cyg (e.g., Mikołajewski et al 1990a, Hoard 1993, Rodgers et al. 1997, Ezuka et al. 1998). For this light curve we find $s/s_{exp} = 19.4$, an unequivocal detection of variability. We did not find any new objects with this level of variability. An analysis of the variability properties of the five previously-known, large-amplitude flickerers is given in Sokoloski et al. (2001b). The bottom panel of Figure 6 shows a marginal detection of flickering in the light curve of survey object CM Aql. In this case, $s/s_{exp} = 1.4$, and we are at or near our limits of detectability. Because of its small amplitude, this variability in this light curve could possibly be due to some unidentified systematic error. Measured and expected variances for the detections and marginal detections of variability are listed in Table 5.

4.2 Periodic Variability

The main tool we used to search for periodic variability was Fourier analysis of the light curves. In the discussion that follows, we consider a light curve that is simply a series of source count values (i.e., not ratios of source and comparison star count values), but the results apply for differential light

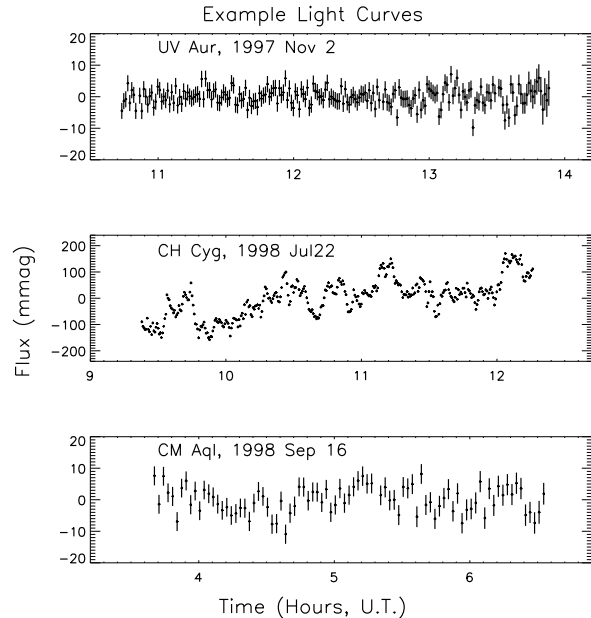


Figure 6. Example light curves showing, from top to bottom, a non-detection, a clear detection, and a marginal detection of rapid variability.

curves as well. Our observations consisted of data points that were at least approximately evenly spaced, so we were able to use a simple discrete FFT routine for this analysis.

Consider a power spectrum constructed using the Leahy et al. (1983) normalization:

$$P_j \equiv \frac{2}{C_{tot}} |a_j|^2, \quad j = 0, \dots, \frac{N}{2}, \quad (18)$$

where $C_{tot} = \sum_{k=0}^{N-1} c(k)$ is the total number of source counts in a light curve ($c(k)$ is the number of source counts in exposure k) and the a_j are the Fourier amplitudes for the set of frequencies $\nu_j = j/(N\Delta t)$,

$$a_j = \sum_{k=0}^{N-1} c(k) e^{2\pi i j k / N} \quad j = -\frac{N}{2}, \dots, \frac{N}{2} - 1 \quad (19)$$

(Δt is the time between data points). Note that $a_0 = C_{tot}$. With this normalization, the average value of the power from from a time series of purely Poisson noise is 2 (see Appendix A). If a light curve consists of a constant plus pure Poisson noise, then the underlying noise in the power spectrum normalized as defined above is distributed like χ^2 with 2 degrees of freedom (van der Klis 1989; see Groth 1975 for derivation). One can therefore integrate the χ^2 distribution to find the probability that a noise power will exceed the power level P in a given frequency bin:

$$\Pr(P_{j,noise} > P) = \frac{1}{2} \int_P^\infty e^{-y/2} dy = e^{-P/2}. \quad (20)$$

Many other types of noise also produce a χ^2 distribution of the noise powers (van der Klis 1989). In the general case of single or multiple noise sources which are normally distributed, the distribution function of noise powers can be written as

$$f(y) = \frac{1}{\bar{P}} e^{-y/\bar{P}}, \quad (21)$$

so that a more general expression for the probability that a noise power will exceed the power level P in a given frequency bin is

$$\Pr(P_{j,noise} > P) = \frac{1}{\bar{P}} \int_P^\infty e^{-y/\bar{P}} dy = e^{-P/\bar{P}} \quad (22)$$

(Groth 1975; Scargle 1982), where \bar{P} is the average noise power near the frequency ν_j .

When examining an entire power spectrum, however, we are no longer asking about the chance of a noise power exceeding a given power P in a particular frequency bin, but instead the chance of a noise power exceeding P in any bin. Since the probability that the power in a given frequency bin will not reach the level P is $1 - e^{-P/\bar{P}}$, the probability that none of the points in the power spectrum will reach power P is $(1 - e^{-P/\bar{P}})^{n_{freq}}$, where n_{freq} is the number of frequency bins. The analogous expression to equation (22) for a multiple frequency bin search is therefore

$$\Pr(P_{noise} > P) = 1 - \left(1 - e^{-P/\bar{P}}\right)^{n_{freq}}, \quad (23)$$

where $\Pr(P_{noise} > P)$ is the probability that at least one of the noise powers will exceed P . Note that in the limit where $e^{-P/\bar{P}}$ is small, this probability for obtaining a noise power greater than P approaches the more intuitive $n_{freq} \times e^{-P/\bar{P}}$.

If a power spectrum computed from one of our survey light curves contained a peak that had less than a 5% chance of having been produced by statistical noise, then that observation was flagged as a potential detection of periodic variability. In other words, if $\Pr(P_{noise} > P) < 0.05$, then there was a 95% chance that a peak in a power spectrum was due to intrinsic source variability. By choosing a confidence level of 95% for the detection threshold, our set of light curves could have produced several spurious detections. This fairly low detection threshold was selected so that real signals were unlikely to be missed, and because follow-up observations could be performed fairly easily (e.g. as were done for Z And; see Sokoloski & Bildsten 1999).

Whereas one can easily evaluate the likelihood that a detected power-spectrum peak is due to intrinsic source variability using the expressions above, the absence of a statistically significant peak is slightly more difficult to interpret. To see what sort of upper limits we can place on the amplitude of a periodic signal, if no significant power-spectrum peak is present, we calculate our sensitivity below, based on the treatment of this subject in van der Klis (1989).

The smallest-amplitude signal to which we are sensitive corresponds to a power $P_{sensitive} = P_{det} - P_{exceed}$, where P_{det} is the minimum power for a secure detection of true source variability, and P_{exceed} is a low value that is very likely to be exceeded by a noise power. Setting the probability in equation (23) to a small number ϵ , we get $P_{det} = -\bar{P} \ln[1 - (1 - \epsilon)^{1/n_{freq}}]$. Setting the probability in equation (22) to a large value $1 - \delta$, gives $P_{exceed} \equiv -\bar{P} \ln(1 - \delta)$. Putting these two expressions together, we find

$$P_{sensitive} = \bar{P} \ln \left[\frac{1 - \delta}{1 - (1 - \epsilon)^{1/n_{freq}}} \right], \quad (24)$$

with $1 - \delta$ and $1 - \epsilon$ both taken to be large (i.e., close to

1). It can be shown that the amplitude, A , of a sinusoidal signal is related to the square of the Fourier amplitude for the bin containing the signal frequency by the expression

$$|a_j|^2 = \alpha \frac{1}{4} A^2 N^2, \quad (25)$$

where α has an average value of 0.77 and depends upon the location of the signal frequency in the frequency bin (van der Klis 1989). Substituting $|a_j|^2 = (P_{sensitive} C_{tot})/2$ (from equation 18, for the Leahy normalization) and solving for A , we find

$$A_{sensitive} \approx 1.14 \frac{\sqrt{C_{tot}}}{N} \ln \left[\frac{1 - \delta}{1 - (1 - \epsilon)^{1/n_{freq}}} \right]. \quad (26)$$

Plugging in some typical numbers and taking $1 - \delta = 1 - \epsilon = 0.95$, we find that in theory we are sensitive to sinusoidal signals with a fractional amplitude

$$\frac{A_{sensitive}}{\bar{c}} \approx 0.001 \left(\frac{C_{tot}}{5 \times 10^7} \right)^{-1/2}, \quad (27)$$

for $N = 200$ and $n_{freq} = 100$ (recall that \bar{c} is the mean value of the number of source counts, c , from a series of measurements). This fractional amplitude is roughly equal to 1 mmag.

Since the power of a sinusoidal signal with a given amplitude depends upon the location of the signal frequency within a frequency bin, the signal amplitude to which we are sensitive is only approximately given by the expression above. Thus, the best way to determine a signal amplitude upper limit when there are no significant peaks in the power spectrum is through simulations. For each light curve, we therefore added sinusoidal variations with a range of amplitudes, frequencies, and phases to the data, and computed the power spectra. The trial frequencies ranged from the Nyquist value to $3/T_{tot}$ for each light curve, where T_{tot} is the total length of a light curve. Using 10^4 realizations for each trial amplitude (100 trial frequencies, and 100 phases for each frequency), we took the signal amplitude upper limit to be that which produced a 95% confidence level detection 95% of the time. The periodic variability upper limits for each object for which no significant peaks were present in the power spectrum are listed in Table 4.

4.3 Sources of Error

To determine the amount of systematic error in our differential photometry, we examined the comparison stars in multiple fields to determine whether there was a systematic excess variance beyond that expected from the CCD equation and scintillation. For star m in image i (out of N images in an observation), the expected fractional variance is given by

$$s_{exp,m}^2(i) = \left(\frac{\sigma_{CCD,m}(i)}{c_m(i)} \right)^2 + s_{scint}^2, \quad (28)$$

where $\sigma_{CCD,m}^2(i)$ is the variance from equation (6) for star m in image i , $c_m(i)$ is the number of stellar counts for star m in image i , and s_{scint} is the scintillation given by equation (10). If the ratio of the fluxes of two stars l and m is formed to remove the effects of clouds and seeing variations, the expected fractional variance of this ratio is

$$s_{exp,lm}^2(i) = s_{exp,l}^2(i) + s_{exp,m}^2(i). \quad (29)$$

The average expected fractional variance for this flux ratio for the entire observation is

$$s_{exp,lm}^2 = \frac{\sum_i \left(\frac{1}{s_{exp,lm}^2(i)} s_{exp,lm}^2(i) \right)}{\sum_j 1/s_{exp,lm}^2(j)} = \frac{N}{\sum_j 1/s_{exp,lm}^2(j)}. \quad (30)$$

For every possible pair-wise combination of comparison stars in the test fields, the flux ratio was formed, the expected fractional variance from the CCD equation and scintillation was calculated, and the actual fractional variance of the flux ratio was measured. By solving a simple system of equations that had the same form as equation (29), we could then obtain the variance due to systematic errors for each star individually.

In most cases, little systematic error was found. Furthermore, the examination of measured versus expected rms variation for constant-brightness field stars allowed us to come up with a criterion for identifying low-level, flickering-type source variability. The constant comparison stars generally had variances that were within 40% of the expected values (both measured and expected variances were typically on the order of a few mmag). Therefore, any symbiotic in the survey with $s/s_{exp} \geq 1.4$ was considered to have a potential detection of variability.

Looking at the comparison-star fluxes with respect to each other in each field also allowed us to identify any variable comparison stars and exclude them from the analysis. Data from a new pulsating A-type star with a 30-minute period that was discovered in this way, as well as several other serendipitous discoveries, are presented in (Sokoloski et al. 2001a).

As mentioned above, we found that in most cases, systematic error was negligible. However, there were a few instances in which problems arose. The first problem we found was a result of the poor centroiding performed in the IRAF-based IDL routine “cntrd”. The centroiding problems are evident from the large scatter in the difference between stellar positions output from “cntrd” for a series of images of the same field. Improved centers were obtained by assuming the PSFs had a roughly bivariate Gaussian shape, and fitting the PSFs with this function with the x and y centers as free parameters. Figure 7 shows a differential light curve for comparison stars in the field of BX Mon on 1997 Feb 26, first before, and after the centering improvement.

A second source of error, “pixelization noise”, is only relevant for small extraction apertures. This error arises because of imperfect estimation of the fraction of counts that should be included from a bin that falls only partially within the extraction region. For large apertures, there are relatively few edge bins compared to bins that are fully within the aperture, and the effect of pixelization is small. To estimate the magnitude of pixelization noise for various aperture sizes, and for stellar PSF profiles of various widths, we created very finely sampled Gaussian stellar profiles, and binned them as they would be on our CCDs, with the true center of the profile placed at 2.5×10^5 different positions in a bin. We then performed circular-aperture photometry with our software for each different PSF position. In Figure 8, several contour plots show the change in extracted flux as a function of position of the PSF center within a bin. In Figure 9 is plotted the fractional variation in the extracted

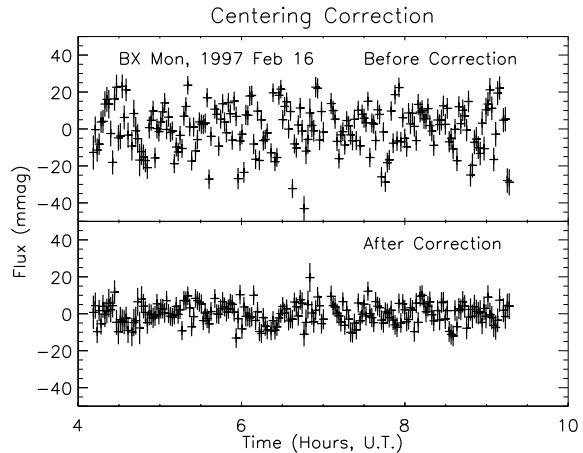


Figure 7. A particularly extreme example of the improvement in our light curves once a centering correction was applied. These light curves were constructed from the 8 comparison stars in the field of BX Mon on 1997 Feb 16, using an aperture radius of $2.9''$.

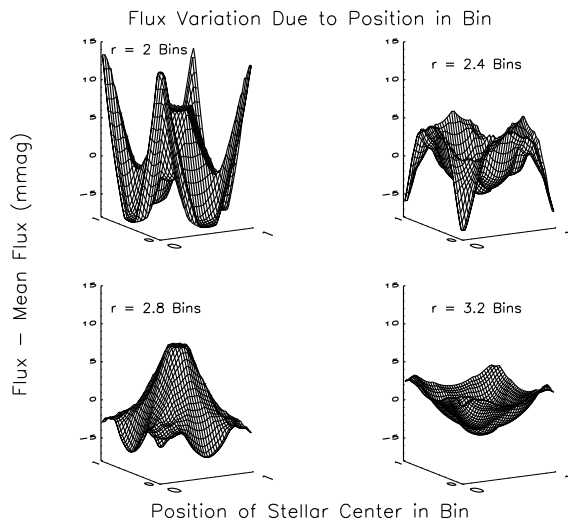


Figure 8. Four examples of the extracted flux as a function of position of the stellar PSF center in a bin. Plotted is the difference in flux from the mean value in units of mmag, for a Gaussian point-spread function with $\sigma_{Gauss} = 1.4$ bins. Note that the variation is smaller for larger extraction radius, r .

fluxes as a function of extraction aperture for various Gaussian profile widths.

Furthermore, there appears to be a slight positional dependence of the PSF (at least for CCD 2), which can be seen by comparing the x and y width of the Gaussian fits for the different stars in a field. For observations with stable seeing, this PSF difference is not a problem. If the seeing changed significantly during an observation, however, then one of the assumptions of our differential photometry was violated, and the light curve could exhibit variability that was either directly or inversely correlated with seeing. It is also possible that excess variance in the final ensemble average light curve could be due to some cosmic rays within the program star extraction region. We were more cautious

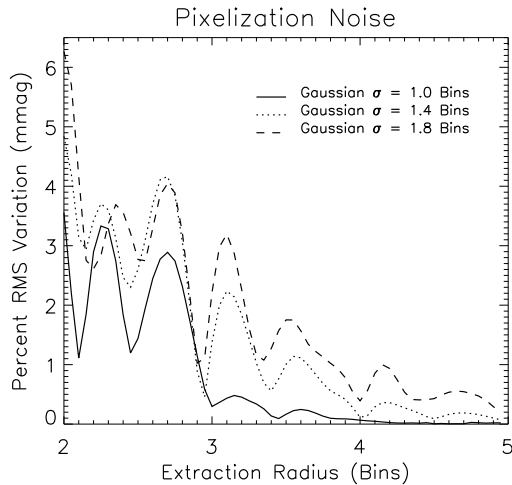


Figure 9. Simulated “pixelization noise” for a range of PSF widths and extraction radii. For CCD 2, 1 bin is equal to $0.74''$, and for CCD 5, 1 bin is equal to $0.59''$. A point spread function with $\sigma_{Gauss} = 1.4$ bins on CCD 2 therefore corresponds to “seeing” of about $2''$.

about removing data with suspected cosmic ray hits on the program star than we were with data in which the comparison stars were affected, in order to avoid removing real variability. However, the numerous light curves for which we do not find excess variability in the program star indicate that this is probably not a significant issue.

In a few observations, a correlation between the differential light curve and a measure of the seeing, the position of the stars on the chip, features seen in the raw light curves of all stars in the field, the background, or some other house-keeping information indicated the possible presence of some systematic error. Likely candidates for the source of the error include differences in the PSFs, blended images, differential extinction, or positional dependences of gain or bias features (see Gilliland & Brown 1988, who find that color and position corrections matter). Any data that were clearly affected by systematic error (usually during extremely poor weather) were not used, and some questionable cases are discussed later. For most observations, however, all of the above effects were small compared to statistical noise sources such as Poisson noise due to counting statistics and read noise.

5 RESULTS

5.1 Upper Limits

For 25 of the 35 objects in our survey, no variability, either periodic or aperiodic, was detected. The fractional rms variations (s) for these objects are listed in Table 4. Some representative light curves and corresponding power spectra are shown in Figure 10. The value of s for these 25 objects ranged from 2.4 to 10.4 mmag, giving $s/s_{exp} \leq 1.4$ (where s_{exp} is the rms fractional variation expected from Poisson statistics and scintillation, defined in equation 15) for all but one observation, which we discuss below. The upper limits on the amplitude of any periodic oscillations

present in these data fall in approximately the same range of a few to 10 mmag, or less than a 1% flux variation (see Table 4). As discussed in §4.2, the oscillation-amplitude upper limits correspond to the amplitude of a sinusoidal signal which, when injected into the data at a range of periods and phases, produced a formal 95% confidence detection 95% of the time.

Two of the observations presented in Table 4 as upper limits actually contained some low-level variability, which we do not believe to be due to intrinsic source variations. The power spectrum from the 1998 Sep 15 observation of AX Per has a peak above the formal signal-detection level. However, significant low-frequency power was also seen in some of the comparison stars as well as AX Per, and so systematic effects were probably present. In the 1997 Jun 7 observation of AG Dra, which was done with only a single comparison star, the flux appears related to the position of the star on the chip, and the variation is therefore also believed to be due to a systematic effect. In both cases, a second observation showed no variability.

The main result for the 25 objects listed in Table 4, and therefore one of the main results from our 35-object survey, is that although most SS contain accreting WDs, as in cataclysmic variables, they generally do not show CV-like optical flickering. For over 70% of the symbiotics in this survey, the amplitude of any rapid optical variability is constrained to just a fraction of a percent.

5.2 New Candidate Flickerers

In 4 systems, evidence for aperiodic rapid variability was found for the first time. We consider an observation to contain a potential detection of rapid variability if $s/s_{exp} \gtrsim 1.4$, and the variations are not correlated with any of our house-keeping data. Since all of these measurements are near our detection limits, however, they should be considered rather uncertain, and further observations are needed to confirm the presence of flickering in these objects. The candidate variable systems are discussed individually below. Their expected and measured fractional rms variations are listed in Table 5.

5.2.1 EG And

EG And was observed on 4 occasions, 3 times with a U filter, and once with a B filter. In 2 of the U -band observations, on 1997 Jul 9 and 1998 Sep 16, there is evidence for low-level flickering. The measured variance was 50% above the expected level on 1997 Jul 9, and more than twice the expected level on 1998 Sep 16. The observation that produced the most variable light curve, on 1998 Sep 16, however, was performed using the smaller-field CCD 5, which only allowed for one reasonably bright comparison star. Moreover, this one bright comparison star was near a feature on the chip which introduced a slow rise in the comparison star flux as the star drifted toward the feature. There does not appear to be a correlation between the position of the comparison star and the rapid flux variations in the light curve, but the presence of this chip feature does introduce another reason for caution when interpreting these results. Plots of the four EG And light curves are shown in Figure 11. The power spectrum

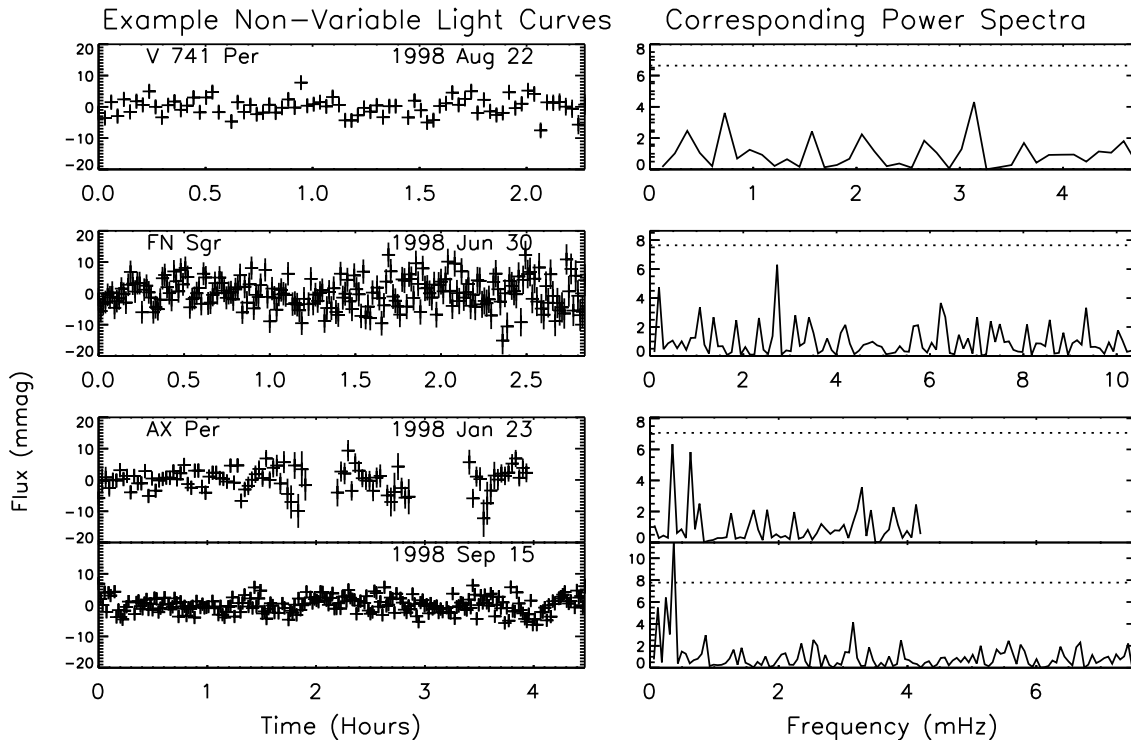


Figure 10. Example light curves and power spectra for several non-variable survey objects. All the non-variable objects are listed, with their variability upper limits, in Table 4. The flux is in units of mmag, and the observations were done with a B filter. The power is normalized by the mean value for an observation, and the dotted line in the power-spectrum plots indicates the power needed for a 95% confidence level signal detection. For the 1998 Sep 15 observation of AX Per, a peak in the power spectrum rises above the formal detection level, but we do not believe this peak is due to intrinsic source variability. This type of observation is discussed in the text.

from 1998 Sep 16 contained significant low-frequency power spread over several frequencies. No statistically-significant peaks were present in the power spectra from the other three observations.

To illustrate the difficulty with interpretation of these observations, Figure 12 shows, for 1998 Sep 16, the flux ratio of EG And flux versus the main comparison star, the flux ratio of EG And flux versus the sum of 2 very faint star in the field, and the flux ratio of the main comparison star versus the sum of the 2 faint stars. For a high-confidence-level detection, one would like to see significant and correlated variability in both the first and second ratios, but not the third. The measured variance is in fact more than twice the expected variance ($s/s_{exp} = 2.4$) for the first ratio, the measured variance is approximately 40% higher than that expected from a constant source for the second ratio ($s/s_{exp} = 1.4$), and the 2 quantities are nearly the same for the third ratio ($s/s_{exp} = 1.1$). For this object, it is also interesting to note that the very flat B light curve of 1997 Jul 11 is only 2 nights away from a U observation that shows hints of variability.

5.2.2 BX Mon

Our first observation of BX Mon, on 1997 Jan 18, produced only a small amount of low-quality data, so we re-observed this object on 1997 Feb 16. On that date, we found a significant excess variance. The rms fractional variation is 2.7

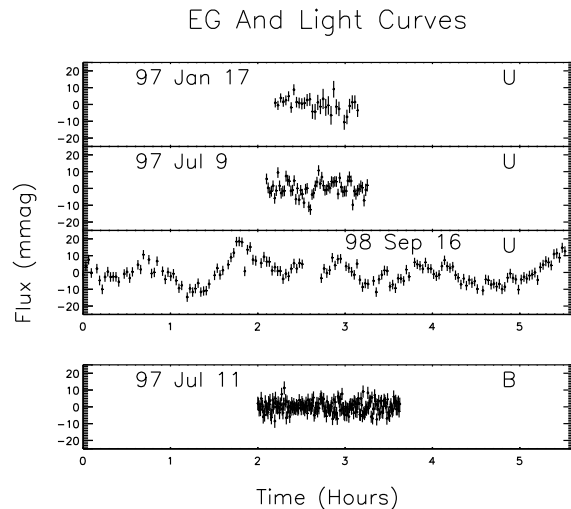


Figure 11. Light curves from the 4 observations of EG And are shown. Statistically significant variability is seen in the second and third U -band light curves, whereas the B -band light curve is consistent with an assumption of constant flux.

times higher than expected from Poisson fluctuations and scintillation. No comparison stars showed similar variations, and the variations in BX Mon were evident no matter what combination of comparison stars was used. Unfortunately,

Table 4. Variability Upper Limits

Name	Date (m/d/yr)	s_{exp} (mmag)	s (mmag)	Max Sine Amplitude (mmag)	Period Range (min)
AX Per	1/23/98	2.8	3.2	4.1	3.9 - 78.6
	9/15/98 ^a	1.9	2.6	1.9	2.2 - 88.9
V 741 Per	8/22/98	2.4	2.8	3.2	3.5 - 45.6
S 32	3/13/97 ^b	7.0	8.2	13	3.1 - 27.0
	9/14/98 ^a	2.7	3.2	3.8	3.2 - 45.0
UV Aur	11/2/97	2.7	2.7	1.9	1.8 - 62.7
TX CVn	3/13/97 ^b	3.2	4.4	4.7	2.9 - 63.5
RW Hya	2/18/97	3.4	4.2	3.6	1.8 - 41.2
BD-21.3873	5/14/97	3.1	3.5	4.6	3.8 - 40.5
	5/31/98	4.7	6.1	7.3	3.0 - 36.2
AG Dra	6/7/97	3.9	6.3	4.7	1.6 - 66.5
	7/23/98	5.4	5.8	4.0	2.7 - 92.9
HD 154791	8/4/97	9.7	10.4	4.6	1.1 - 96.9
Hen 1341	6/28/98	3.3	3.1	3.1	3.1 - 46.6
AS 289	5/31/98	6.2	7.7	9.8	3.7 - 51.9
YY Her	5/14/97	5.4	5.3	4.0	2.5 - 76.9
AS 296	8/21/98	2.3	2.4	2.5	3.8 - 61.4
S 149	5/15/97	3.5	3.8	3.8	2.8 - 44.7
	8/20/98	3.6	3.4	2.5	2.6 - 91.5
V 443 Her	4/7/97	2.8	2.7	2.5	2.6 - 55.2
FN Sgr	6/30/98	3.9	4.6	3.3	1.6 - 56.5
V 919 Sgr	8/22/98	3.0	3.0	3.2	3.9 - 49.3
CI Cyg	6/8/97	3.7	4.0	2.6	1.5 - 61.3
	9/15/98 ^a	3.9	5.4	5.8	4.2 - 87.5
AS 360	6/29/98	3.4	4.8	4.7	2.6 - 46.8
PU Vul	6/15/97	3.1	3.8	5.1	2.0 - 27.4
He2-467	8/22/98	2.5	2.4	2.9	3.9 - 42.2
S 180	7/23/98	5.5	5.5	11	4.2 - 30.1
S 190	8/21/98	3.7	4.5	3.4	2.2 - 68.6
AG Peg	9/17/98 ^a	2.9	3.5	7.3	1.6 - 50.4
R Aqr	9/14/98 ^a	4.6	5.4	3.4	1.7 - 78.1

^a The timing errors are larger than usual for observations done in 1998 Sep because the high precision WWVB clock was broken. For these observations, the time between integration starts is uncertain by up to a few seconds.

^b On 1997 Mar 13, incorrect time stamps were recorded in the image headers. The timing for this date is therefore only approximate.

there is some chance that these variations are due to atmospheric changes. A plot of seeing as a function of time looks similar to the BX Mon light curve in places, although the two quantities are not strictly correlated. The 1997 Feb 16 light curve for BX Mon, and a measure of the PSF width (from a different star in the same field) during the observation, are shown in Figure 13. The seeing measure plotted in this figure is the second moment of the distribution of counts within the aperture used.

Follow-up observations were performed in 1997 Mar, Apr, and Nov, but the results for this object remain inconclusive. Flickering was possibly detected in a *U*-band observation on 1997 Mar 12 ($s/s_{exp} = 1.9$), but on this night some of the comparison stars also showed excess variability. Variations were not detected in any other observations. Example light curves, from 1997 Mar 12 and 1997 Nov 1, are shown in Figure 14.

5.2.3 CM Aql

We observed CM Aql once, on 1998 Sep 16, with a *B* filter, using CCD 5. The measured fractional variation is just 35% higher than expected for this observation (i.e., $s/s_{exp} = 1.35$). However, the small variations that are present (see Figure 15) do not appear related to any of our house-keeping data, and the observation was done in good weather conditions. This situation is in contrast to other borderline case observations with $s/s_{exp} \approx 1.4$ (e.g., TX CVn, CI Cyg, and AS 360), which were done under poor weather conditions or do not show any point-to-point correlated variations. Further observations are required to determine whether this flickering is intrinsic to CM Aql. It is possible that the higher-sensitivity CCD 5 requires a more thorough study of systematic effects.

Table 5. Candidate Variable Systems

Name	Date (m/d/yr)	Filter	Fractional Variation			Power Spectrum	
			s_{exp} (mmag)	s (mmag)	s/s_{exp}	Max. Sine Amplitude (mmag)	Period Range (min)
EG And	1/17/97	<i>U</i>	3.7	3.8	1.0	6.9	3.6 - 19.3
	7/9/97	<i>U</i>	3.2	4.7	1.5	5.8	2.2 - 23.2
	7/11/97	<i>B</i>	3.7	3.5	0.9	2.3	0.9 - 32.3
BX Mon	9/16/98	<i>U</i>	2.8	6.7	2.4	Low-frequency power present	
	1/18/97 ^b	<i>B</i>	10.2	9.1	0.9	-	-
	2/16/97	<i>B</i>	3.7	9.9	2.7	Low-frequency power present	
	3/12/97	<i>U</i>	6.8	13.1	1.9	Low-frequency power present	
	4/7/97	<i>B</i>	4.5	6.0	1.3	10.2	2.8 - 19.7
CM Aql	11/1/97	<i>B</i>	3.9	4.2	1.1	4.3	3.4 - 51.1
BF Cyg	9/16/98 ^a	<i>B</i>	3.1	4.2	1.4	4.3	4.0 - 57.6
	4/6/97	<i>B</i>	4.1	9.2	2.2	Low-frequency power present	
BF Cyg	7/11/97	<i>B</i>	3.6	7.8	2.2	Low-frequency power present	
	7/1/98	<i>B</i>	2.5	5.5	2.2	Low-frequency power present	

^aTiming errors are larger than usual on this date because the high-precision WWVB clock was broken.

^bToo little data to compute meaningful power spectrum.

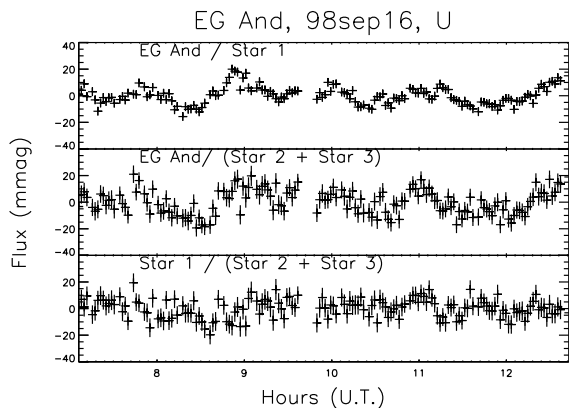


Figure 12. Flux ratios for EG And and other stars in the same field. For a secure detection of variability in EG And, the light curves in the first 2 panels should show the same trends, while the light curve in the third panel should not. Based on these light curves, we classify this observation as a marginal detection of variability in EG And.

5.2.4 BF Cyg

We found low-amplitude variability in BF Cyg on three separate occasions, separated by more than a year. This variability does not appear to be correlated with seeing or any other house-keeping data, and it was not seen in any of the 5 comparison stars. In each observation, the measured variance was more than twice that expected from Poisson variations and scintillation ($s/s_{exp} > 2$), and so this source is a prime candidate for follow-up study. All observations were done with the *B* filter. The light curves are presented in Figure 16.

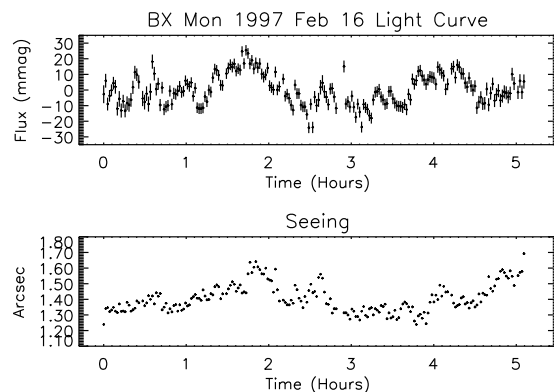


Figure 13. Light curve and seeing measure for the 1997 Feb 16 observation of BX Mon. Rapid variability is detected, but its origin is questionable. The variations could either be intrinsic to BX Mon, or possibly due to atmospheric changes that were imperfectly subtracted out by the differential photometry. See text for details.

5.3 Previously-Known Flickering Symbiotics

Included in our survey were five well-known flickering symbiotics: Mira AB, MWC 560, T Crb, RS Oph, and CH Cyg. We confirmed the presence of rapid optical variability in all five systems, and recorded a marked change in the flickering properties of both T CrB and CH Cyg over the course of the survey. A full analysis of these observations is presented elsewhere (Sokoloski et al. 2001b), but example light curves for each of the large-amplitude flickerers are shown in Figure 17. These light curves are shown, at least in part, to emphasize the difference between these five systems and the other 30 objects in the sample. Note that the ordinate

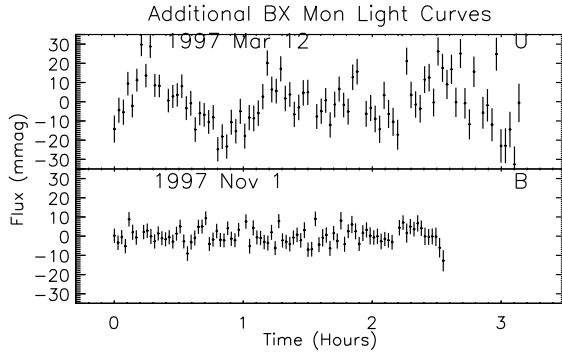


Figure 14. Example light curves for BX Mon. Rapid variability is marginally detected in the U -band observation on 1997 Mar 12 (top panel), but not in the B -band observation on 1997 Nov 1 (bottom panel).

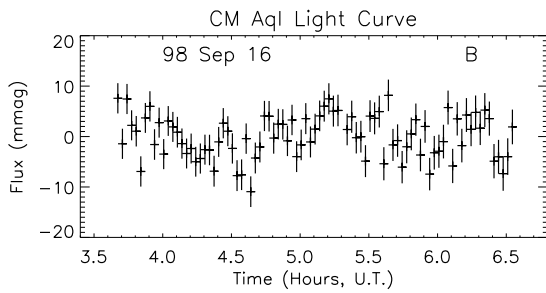


Figure 15. B -band light curve for CM Aql. This observation is right at the border between a non-detection and a marginal detection of rapid variability.

for each plot in Figure 17 spans 0.5 magnitudes, whereas the 25 objects for which no rapid variations were detected are constant to within a few mmag. The four new candidate flickerers vary at a level of only a few tens of mmag.

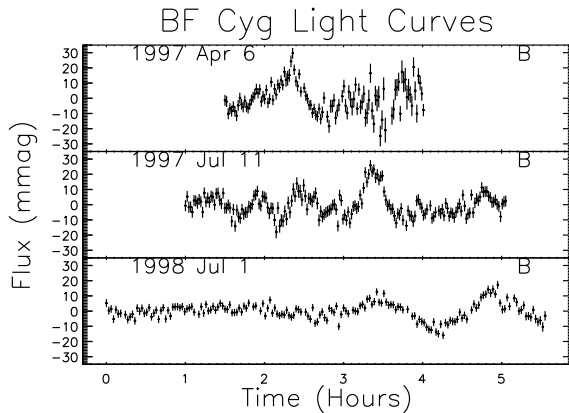


Figure 16. B -band light curves for BF Cyg.

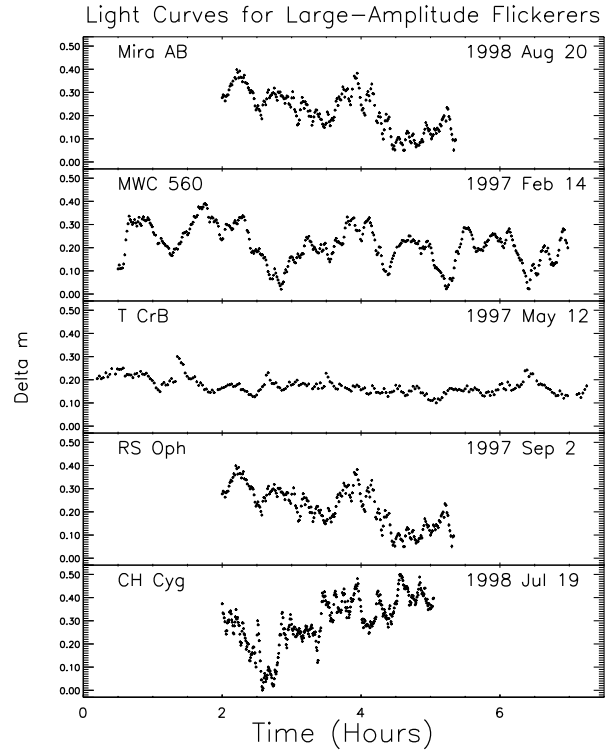


Figure 17. Representative B -band light curves for the previously-known flickering symbiotics. These objects form a subclass of symbiotics that are clearly distinct from the majority of systems, in which rapid optical variability either has very low amplitude or is undetectable.

5.4 Future Work

Although for the faintest targets a larger telescope would have improved our sensitivity, in most cases we were more limited by the capabilities of the CCD detectors than the telescope collecting area. The limitations of the CCDs were especially apparent for the bright objects, objects with bright comparison stars, or objects in sparse fields. When we observed fields containing bright stars, integration times were limited by CCD non-linearity and saturation, and the duty cycle of an observation was sometimes low. To improve measurements of low-amplitude rapid variability, one would like to have a CCD with a larger field of view and faster readout times. Masking techniques in which part of the CCD is read out while another part is exposed would greatly improve the efficiency of this type of observation. A larger field would allow for additional bright comparison stars. For some objects with no moderately bright stars nearby, this improvement is absolutely essential for differential photometry. For other fields, having a larger number of comparison stars would allow for point-spread-function fitting and a better understanding of systematics. In addition, the ideal detector would have either a variable gain, or a gain that was high enough to allow for photometry on a field of stars with a large dynamic range of brightnesses. One would like to always have the option of integrating to the scintillation limit before saturating a star or reaching the non-linear regime. With such a detector, and observations

done at low airmass, one could probe much lower levels of variability (< 1 mmag), as well as shorter time scales.

6 DISCUSSION

Our survey has revealed new hints of rapid variability in four symbiotics: EG And, CM Aql, BX Mon, and BF Cyg. Our main result, however, is that most symbiotics do not vary on a time scale of minutes, down to a level of mmag. Previous authors have noted this apparent general lack of rapid variability in symbiotics (e.g. Walker 1977; Dobrzycka et al. 1996). Our work broadens and strengthens this conclusion. We have placed tight upper limits on both aperiodic and periodic variability for 25 of the 35 objects observed. We also performed extensive observations of the five previously-known large-amplitude flickerers, which are found to be rare among symbiotics. These observations, as well as serendipitous discoveries of five new variable stars and results for the magnetic symbiotic Z And, are presented in separate papers (Sokoloski & Bildsten 1999; Sokoloski et al. 2001a; Sokoloski et al. 2001b).

This survey of optical variability has been carried out primarily in the *B*-band, with some supplementary observations done in *U*. The *B*-band optical flux from symbiotics originates from several sources, including the red giant, recombination radiation from the nebula (which is pumped by the far-ultraviolet and soft X-ray emission from the hot component), and possibly some direct emission from a disk or the hot star itself. For comparison, the optical flux in CVs is dominated by emission from the accretion disk, and in supersoft sources the optical light is primarily from an irradiated disk. We discuss below the differences in optical variability properties between symbiotics and other accreting-WD binaries, differences among the SS, and what these variability properties might be telling us about the underlying sources of light.

One of the important distinctions between CVs and symbiotics is that in many symbiotics, the high hot-component luminosity indicates that material must be burning quasi-steadily on the surface of a white dwarf, either because the accretion rate is in the steady-burning regime, or as residual burning from a past outburst (Paczynski & Rudak 1980; Iben 1982; Mikołajewska & Kenyon 1992; Sion & Starrfield 1994). Some of the far-ultraviolet and soft X-ray flux from this persistent nuclear burning is reprocessed into the optical by the nebula. Since the flux from the nuclear burning does not change on short time scales, and the nebula itself is unlikely to introduce rapid variability, the nuclear burning produces an extra contribution to the optical flux in symbiotics that is not variable on short time scales. Therefore, the amplitude of any rapidly variations from the accretion are reduced compared to similar variations in CVs. In supersoft sources, as in symbiotics, far-ultraviolet and soft X-ray emission from nuclear burning on a WD is reprocessed into the optical. In supersoft sources, however, the reprocessing occurs primarily in a flared accretion disk instead of an extended nebula (Popham & DiStefano 1996), and disk-rim fluctuations could introduce an additional source of rapid optical variability (Meyer-Hofmeister et al. 1998).

Thus the amplitude of rapid optical variability in symbiotics and other accreting-WD binaries is linked to the pres-

ence or absence of a physical process (nuclear burning) that profoundly affects the binary. Nuclear burning on the surface of a WD produces much more power than accretion alone, and the presence of such burning may be closely related to the outbursts in classical symbiotics. In one model for these outbursts, the months-to-years-long events are due to the expansion of the white dwarf photosphere in response to an increase in the accretion rate onto the WD (see Mikołajewska & Kenyon 1992 for a review of these models). But this phenomenon, which is similar to that proposed to explain the optical rises and X-ray dips of the supersoft sources (e.g. Kahałka 1998), can only occur if the WD is burning material quasi-steadily. And there is another reason why it is critical to understand how the accumulated fuel is burning. Symbiotics might be progenitors of Type Ia supernovae, but this depends on their ability to increase in mass as they accrete. The more fuel that is burned in steady-state, the better for increasing the mass of the WD, since large classical nova outbursts can actually excavate the WD. The connection between the amplitude of rapid optical variability and the presence of nuclear burning on the WD is explored in greater detail in section §6.3.

6.1 Magnetism in the Accreting White Dwarfs

In our survey of 35 symbiotics, we found one new clearly magnetic system (Z And; see Sokoloski & Bildsten 1999). For 25 objects, we detected no rapid variability, and we place upper limits ranging from 1.9 to 13 mmag on periodic oscillation amplitudes in these objects. The absence of a detected periodic signal in these 25 systems, however, does not necessarily mean that they are not magnetic. The amplitude of the Z And oscillation during quiescence was extremely small (roughly 1 mmag peak-to-peak), and the presence of a similar-sized oscillation in the other objects is not ruled out by any of the upper limits in Table 4. In fact, the Z And oscillation was only discovered because the object was fortuitously observed during an outburst of the system, during which the oscillation amplitude was larger. It is worth noting here that estimates of the luminosity of the WD in Z And gives values of 500 - 2000 L_{\odot} (Mürset et al. 1991; Dobrzycka et al. 1996, and references therein), indicating that nuclear burning must be occurring on the surface of the WD. Given our discussion above concerning the affect of nuclear burning on the amplitude of rapid optical variations, it is not surprising that the amplitude of the Z And oscillation is much smaller than the corresponding optical modulations seen in intermediate polars.

Searching for oscillations is more subtle in the flickering objects, and we tackle this problem in a separate paper (Sokoloski et al. 2001b). Therefore, here we only place a lower limit on the fraction of symbiotics in our sample that contain magnetic white dwarfs. Since we detected one magnetic system out of 32 possible WD systems (three symbiotics in our sample have either main-sequence-star or neutron-star hot components), at least 3% of the WD systems in our sample are strongly magnetic. This number should be compared to 2% for field white dwarfs (53 out of 2249; Anselowitz et al. 1999), and 5 - 10% for white dwarfs in CVs (Warner 1995). Although the statistics are obviously too small to determine the true magnetic fraction for SS, our

results are consistent with this fraction being higher than it is in the field, as with CVs.

6.2 Flickering

Our survey did not yield any new strong ($s \gtrsim 20$ mmag) flickerers. For most objects, the upper limit we have placed on aperiodic variability (flickering) is a few mmags (see Table 4). Weak flickering (at the $\lesssim 10$ mmag level) was possibly detected in a few of our survey objects, which we discuss in §5. Unfortunately, flickering at this low level is difficult to attribute to the source, as many observational systematics can have a comparable amplitude. The new candidate flickerers are, however, clearly worth additional study.

By comparing the small fractional rms variations listed in Table 4 and Table 5 with the large flickering amplitudes of the 5 well-known flickering symbiotics shown in Figure 17, it is apparent that the distribution of flickering amplitudes in symbiotics is bimodal; there are a few large-amplitude flickerers, but most symbiotics show little to no flickering. This is in sharp contrast to the CVs, where most show persistent flickering at a level of $\gtrsim 100$ mmag. The flickering light in CVs could come from several areas, including the inner accretion disk, the splash point, or the surface of the WD (Warner 1995; Bruch 1992). Moreover, these flickering sources contribute to different degrees in different object. But no matter which specific origin, the power source is accretion, and flickering is prevalent in the CVs. We have found that flickering is much less prevalent in the symbiotics. Several possible explanations include: (a) the optical flux in most SS is dominated by light from the red giant, which doesn't change on short time scales, (b) the nebula “washes out” the flickering light, (c) most SS do not accrete though a disk, and the wind-fed accretion does not produce optical flickering, or (d) in SS with no, or only small-amplitude, rapid variations, much of the hot component light is from nuclear burning of accreted material, which is stable on a time scale of minutes. We consider each of these possibilities below.

6.2.1 The Red Giant

We can rule out this simple explanation by comparing the red giants in the flickering and non-flickering symbiotics. If the red giants in the flickering symbiotics were systematically fainter, or of later spectral type, than the red giants in the non-flickering symbiotics, the contribution to the B -band flux from the red giant would be lower. This reduced contribution from the red giant could allow any variable emission from the hot component that might normally be hidden to be revealed.

In fact, there is no such systematic difference. Kenyon & Fernandez-Castro (1987) derive spectral types for the giants in 25 symbiotic binaries, and find most systems to be M2-5 III. Included in their study were three of the well-known large-amplitude flickerers (T CrB, CH Cyg, and RS Oph), and two of our marginal flickering detection objects (EG And and BX Mon). The red giant in T CrB is found to be $M4.1 \pm 0.3$ III, that in CH Cyg to be $M6.5 \pm 0.3$ III, and that in RS Oph to be $K5.7 \pm 0.4$ I-II. The red giant in EG And was found to have spectral type $M2.4 \pm 0.3$ II, and

the red giant in BX Mon was found to have type $M4.6 \pm 0.4$ III. These giants are therefore all quite typical for symbiotics, except for that in RS Oph, which is actually earlier and brighter than average. Furthermore, if the contribution from the red giant was the main factor in determining the flickering amplitude, one would expect a more continuous distribution of amplitudes.

6.2.2 The Nebula

Radio observations of thermal bremsstrahlung from the photo-ionized nebulae in SS indicate that typical sizes are usually less than 10^{15} cm (Seaquist et al. 1984). From UV line intensity ratios, densities in the nebula are estimated to be 10^8 to 10^{10} cm^{-3} , and temperatures are on the order of 10^4 K (Kenyon 1986, Nussbaumer & Vogel 1987). The presence of the nebula could make flux modulation from either magnetic accretion or flickering more difficult to detect in SS.

The nebula can affect the rapid optical variability in two ways. Nebular reprocessing can hide some temporal variations from the hot component which originates in the FUV or higher energies by acting as a low-pass filter. In addition, non-variable or slowly varying optical emission from the nebula will reduce the amplitude of any rapid variability that might originate in the optical band, for example from an accretion disk. Rapid variations in the flux of ionizing photons could possibly be passed into the optical if the nebula is dense and radiation bounded (i.e., if the ionized nebula is in the form of a simple closed Strömgren region). Roughly speaking, if the nebula is radiation bounded, far-ultraviolet photons are all absorbed in photo-ionization events. If the output of ionizing photons varies, then the size of the Strömgren region varies, and so does the amount of reprocessed optical light. If the nebula is dense enough at the boundary between the ionized and neutral regions, the recombination time will be short, and rapid variations in the ionizing flux could in principle be propagated into the optical. Typical densities in the red giant winds that form the nebula can reach $\sim 10^{10}$ cm^{-3} , giving a hydrogen recombination time of minutes. However, most SS nebulae are likely not radiation bounded (Mürset et al. 1991). In addition, light travel time effects would cause any sharp temporal features to be smeared out, as this light would be reprocessed in parts of the nebula that are different distances away from the hot white dwarf. Finally, if the reprocessing time in the nebula is long, then the rapid variability will not be passed along to the optical light, no matter whether the nebula is radiation bounded or density bounded (gas completely ionized so that some ionizing photons escape). The ionized nebula does not have as much effect on optical photons, so variability which originates in the optical should not be washed out, only possibly diluted. Given the above discussion about the difficulty of producing rapid variability from the nebular emission, we would expect the spectrum of the rapidly-variable component of the large-amplitude flickerers (such as RS Oph) to reflect the physical origin of the variations, for example in an accretion disk, and not be dominated by nebular features.

6.2.3 Accretion Disk or Not?

An interesting question to ask is whether the amplitude of flickering in SS can tell us whether the accreted material's final plunge onto the WD is via a disk or directly from the wind. The flickering in CVs is related to disk accretion, and Livio (1988) showed that disks might well form in wind-fed symbiotics. A simple reason why disk formation is possible is the large contrast between the accretion radius, $r_a = GM/V^2 \approx 10^{13}$ cm (where V is the relative velocity between the red-giant wind and the WD), and the WD radius, $R \approx 10^9$ cm. In addition to being a known source of flickering in CVs, a disk could naturally reveal much of this flickering in the optical, and as we have mentioned above, optical photons are less affected by the nebula than higher energy ionizing photons. Unfortunately, we have no *a priori* phenomena to invoke to help us know whether or not to expect optical flickering from direct (i.e. no disk) wind accretors. It is possible that material accreted onto a white dwarf directly from an inhomogeneous wind could also produce rapid variability, as is seen from wind accretion onto neutron stars in X-ray binaries. However, the emitted spectrum would not necessarily have a large optical component, and variability from direct, disk-less accretion might therefore be more likely to be hidden.

Although the existence of accretion disks in symbiotics appears likely, there is little direct evidence for disks around WDs in SS. Disks are not needed in spectral fits for most systems (Mürset et al. 1991) and double-peaked line profiles in most cases cannot be definitively linked to disk emission (Robinson et al. 1994). Observational evidence for a disk formed from a wind has been found in Mira by Reimers & Cassatella (1985), and Lee & Park (1999) have inferred the presence of an accretion disk from double-peaked Raman scattering lines in RR Tel. Sokoloski & Bildsten (1999) have suggested that the small outburst of Z And in 1997 is consistent with a disk-instability event, but the inference of a disk there is indirect.

Finally, even if one did have direct evidence of a disk, the presence of a disk does not guarantee the presence of a flickering source of light. Flickering is not seen in some dwarf novae near the maximum of outburst (Warner 1995), possibly due to the high \dot{M} . As we have discussed, symbiotics have higher accretion rates than most CVs, so it is possible that the disks in SS would not flicker to the same extent that CV disks do. In summary, although there are reasons to believe that accretion through a disk and disk-less wind accretion would produce a different level of rapid optical variability, we are not yet at the point of being able to use rapid optical variability as a conclusive diagnostic of the form of accretion.

6.2.4 Nuclear Power versus Gravitational Power, and the relationship between flickering and outbursts

In their study of 8 SS, Dobrzycka et al. (1996) note that the objects with lower hot-component luminosities, L_{hot} , seem more likely to flicker. Our study of 35 objects produced 4 new candidate small-amplitude flickering systems, but showed primarily that most SS do not flicker (i.e., most have variations of less than a few mmag). Could this widespread lack of large-amplitude flickering be due to the source

of power in SS? A potential hint to the flickering puzzle can be found by considering the symbiotic recurrent novae, which clearly burn most of their fuel in outbursts. They are thus unlikely to have large nuclear-burning luminosities in quiescence. The expectation that these systems (between novae) are largely powered by gravitational energy release is consistent with the detected flickering. For example, at least three of the four symbiotic recurrent novae (RS Oph, T CrB, V1017 Sgr; we are not aware of observations of the fourth, V3890 Sgr) flicker, and these three systems also have $L_{hot} < 100 L_{\odot}$ (Dobrzycka et al. 1996). Moreover, the flickering amplitude in these systems is comparable to that seen in CVs (Walker 1977). The other strong flickerers are MWC 560, CH Cyg, and Mira. Both Mira and CH Cyg have low hot component luminosities ($L_{hot} < 10 L_{\odot}$). In MWC 560, the hot component is brighter, but the uncertainty in this quantity is large.

Generally speaking, it is clear that the objects with low L_{hot} preferentially exhibit CV-like flickering. It is also the case that the objects with higher L_{hot} generally either do not flicker, or have only small-amplitude flickering. An interesting speculation that follows from this observation is that any SS that are found to display large-amplitude optical flickering should eventually experience a nova.

A final bit of supporting evidence for the picture in which the amplitude of the rapid optical variations is reduced in SS that contain nuclear burning on a WD is the low amplitude of the coherent oscillation in Z And compared to the DQ Her systems. The optical light of the DQ Hers typically is typically modulated by about 10% at the WD spin period (Warner 1995; Patterson 1994), but in Z And the modulation is only about 0.1% (when the system is in quiescence). This modulation would be expected to be smaller than those seen in the DQ Her systems if there is a large additional source of relatively constant optical flux. Note that this argument is based on the assumption that the amount of pulsed optical flux from accretion onto a magnetic WD is intrinsically the same for the two types of systems, which may not in fact be the case.

6.3 More on Nuclear Burning

Most cataclysmic variables are clearly powered by gravitational energy released in the process of accretion. In these low accretion-rate systems ($\dot{M} < 10^{-9} M_{\odot} \text{ yr}^{-1}$), the nuclear burning of the accreted material occurs via classical novae and very little fuel is burned between nova events. This should be contrasted with the supersoft sources, where the high luminosity and spectral fitting from ROSAT points to steady-state nuclear burning as the prime power source for their emission at all times (van den Heuvel et al. 1992). The required accretion rates for stable burning range from $\dot{M} \approx 10^{-8} M_{\odot} \text{ yr}^{-1}$ for a $M = 0.4 M_{\odot}$ WD to $\dot{M} \approx 3 \times 10^{-7} M_{\odot} \text{ yr}^{-1}$ for a $M = 1.2 M_{\odot}$ WD (Paczynski & Żytkow 1978; Fujimoto 1982).

The white dwarfs in symbiotics are thought to accrete at a rate of $\sim 10^{-8} M_{\odot} \text{ yr}^{-1}$. This rate is in the range that can produce steady burning, and therefore forces us to consider the importance of nuclear burning as an energy source in these systems. For accretion onto a white dwarf, nuclear energy release exceeds that from gravity by a factor of ~ 30 (the ratio of the accretion energy,

$GM/R \approx 100 - 200$ keV *nucleon*⁻¹, to the nuclear burning energy, 5 MeV per nucleon, is 2-3%), so that even partial burning of the accreting fuel can prove important. Indeed, L_{hot} is so high for many symbiotics that gravitational energy release cannot be the sole source of power, and burning must be occurring. Careful spectral analysis of the nebular emission lines in symbiotics is used to infer the luminosity, L_{hot} , of the hot component, which is modeled as either a star or the inner region of an accretion disk (Kenyon & Webbink 1984; Mürset et al. 1991). We show these L_{hot} estimates, where available, in Table 3, along with other properties. Furthermore, some symbiotics have been detected with ROSAT as supersoft X-ray emitters (Mürset et al. 1997). It is not clear, however, that this steady burning consumes all of the accreted fuel; possibly some is still being accumulated and burns in an outburst.

A key point to note here is that the nuclear-burning luminosity would not be expected to change on short time scales such as minutes or hours. Hence, a WD that is steadily burning the accreting material, and reprocessing the burning emission into the optical, cannot flicker rapidly at a high level. The thermal time in a steadily burning envelope at a depth denoted by the mass above it, ΔM , is $t_{th} \approx (C_P T / E_{nuc})(\Delta M / \dot{M})$, where $C_P \approx 5k_B / 2\mu m_p$ is the specific heat at constant pressure (k_B is Boltzmann's constant, and $\mu \approx 1/2$ is the mean molecular weight), T is the temperature in the envelope, and $E_{nuc} \approx 5 \times 10^{18}$ erg g⁻¹ is the nuclear energy released by hydrogen burning. For a typical temperature in a marginally stable burning region of $T \approx 3 \times 10^7$ K, the expression above gives

$$t_{th} \approx 2 \times 10^{-3} \left(\frac{\Delta M}{\dot{M}} \right). \quad (31)$$

For a $1.2 M_\odot$ WD, this time is approximately ten days, using $\Delta M = 3 \times 10^{-6} M_\odot$ from Figure 7 in Fujimoto (1982), and $\dot{M} = 2 \times 10^{-7} M_\odot \text{ yr}^{-1}$. This time scale is shorter for more massive WDs, as ΔM decreases with the mass of the WD. The shortest possible time is thus for a near-Chandrasekhar-mass WD, and even then equation (31) gives a time scale of about one day (for $M = 1.4 M_\odot$, $\Delta M = 4 \times 10^{-7} M_\odot$, and $\dot{M} = 3 \times 10^{-7} M_\odot \text{ yr}^{-1}$). So, it appears that the thermal time at the location where the burning is occurring cannot get shorter than about a day.

In symbiotics, a significant amount of the nuclear burning flux can end up in the optical because of reprocessing in the nebula. Since this flux does not vary rapidly, and the nebula is unlikely to introduce rapid variations, any short-time-scale optical variations due to accretion are like to be hidden or reduced, as we have found. In the supersoft sources, high-energy photons from the nuclear burning can also be reprocessed into the optical, but in these systems it is the large, flared disk that is the site of the reprocessing (Popham & di Stefano 1996). Photometric observations with the required sensitivity are difficult to perform for most supersoft sources, since they are generally fainter in the optical than CVs or SS, but photometric studies have been done. Rapid optical variability was detected in the Galactic supersofts RX J0925.7-4758 (Clarkson et al. 2001), RX J0019.8+2156 (Meyer-Hofmeister et al. 1998), 1E 0035.4-7230 (Crampton et al. 1997; van Teeseling et al. 1998), and possibly several others as well. Meyer-Hofmeister et al. (1998) suggest that the variations in RX J0019.8-2156 are

due to changes in the disk rim, where the nuclear-burning light is reprocessed. The rapid variations in some of the supersofts could also be due to CV-like flickering from the disk that has not been completely hidden by the nuclear-burning light. For information on the effect of nuclear burning in CVs, we can look at the short-period system T Pyx ($P_{orb} = 1.8$ hr). T Pyx is believed to be burning material to a significant extent even in quiescence (Patterson et al. 1998). However, it does not have a nebula or other large reprocessing site where the high-energy photons can be converted to optical light, so the flux from the quasi-steady burning in T Pyx probably makes only a relatively small contribution to the optical flux. In fact, the optical light curves from this system show obvious large-amplitude flickering (Patterson et al. 1998), presumably from the accretion disk. So, in examining the relationship between the optical variability properties of SS and other WD accretors, we find that the presence or absence of nuclear burning on the WD can have an important effect, but that the nature of the reprocessing site is also relevant.

ACKNOWLEDGMENTS

We would like to thank Mike Eracleous, James Graham, and Marten van Kerkwijk for useful discussions, Mike Liu, Jonathan Baker, Greg Ushomirsky, and Ed Brown for assistance with software, and the support staff at Lick Observatory, especially Tony Misch, Rem Stone, and Will Deitch. We also thank the referee Krzysztof Belczyński for his careful reading of the manuscript and useful comments. This research was partially supported by NASA via grant NAG 5-8658 and by the National Science Foundation under Grants PHY94-07194, PHY99-07949 and AY97-31632. L. B. is a Cottrell Scholar of the Research Corporation.

REFERENCES

- Angel J. R. P., Borra E. F., Landstreet J. D., 1981, *ApJS*, 45, 457
 Anselowitz T., Wasatonic R., Matthews K., Sion E. M., McCook G. P., 1999, *PASP*, 111, 702
 Bevington P. R., 1969, *Data reduction and error analysis for the physical sciences*. New York: McGraw-Hill, 1969
 Bruch A., 1992, *A&A*, 266, 237
 Bruch A., Duschl W. J., 1993, *A&A*, 275, 219
 Ciardullo R., Bond H. E., 1996, *AJ*, 111, 2332
 Clarkson W., Charles P. A., Sokoloski J. L., 2001, in preparation
 Crampton D., Hutchings J. B., Cowley A. P., Schmidtke P. C., 1997, *ApJ*, 489, 903
 Dobrzycka D., Kenyon S. J., Milone A. A. E., 1996, *AJ*, 111, 414
 Downes R. A., Keyes C. D., 1988, *AJ*, 96, 777
 Ezuka H., Ishida M., Makino F., 1998, *ApJ*, 499, 388
 Fritz T., Bruch A., 1998, *A&A*, 332, 586
 Fujimoto M. Y., 1982, *ApJ*, 257, 767
 Gilliland R. L., 1992, "Details of Noise Sources and Reduction Processes". *ASP Conference Series 23: Astronomical CCD Observing and Reduction Techniques*, p. 68
 Gilliland R. L., Brown T. M., 1988, *PASP*, 100, 754
 Gilliland R. L., Brown T. M., 1992, *PASP*, 104, 582
 Groth E. J., 1975, *ApJS*, 29, 285
 Hayes D. S., Latham D. W., 1975, *ApJ*, 197, 593
 Hoard D. W., 1993, *PASP*, 105, 1232

Howell S. B., 1992, Introduction to Differential Time-Series Astronomical Photometry. ASP Conference Series 23:Astronomical CCD Observing and Reduction Techniques, p. 105

Iben I., 1982, ApJ, 259, 244

Iben I. J., Tutukov A. V., 1996, ApJS, 105, 145

Kahabka P., 1998, A&A, 331, 328

Kahabka P., van den Heuvel E. P. J., 1997, ARA&A, 35, 69

Kenyon S. J., 1986, "The symbiotic stars". Cambridge and New York, Cambridge University Press, 1986, 295 p.

Kenyon S. J., Fernandez-Castro T., 1987, AJ, 93, 938

Kenyon S. J., Garcia M. R., 1989, AJ, 97, 194

Kenyon S. J., Oliverson N. A., Mikolajewska J., Mikolajewski M., Stencel R. E., Garcia M. R., Anderson C. M., 1991, AJ, 101, 637

Kenyon S. J., Webbink R. F., 1984, ApJ, 279, 252

Leahy D. A., Darbro W., Elsner R. F., Weisskopf M. C., Kahn S., Sutherland P. G., Grindlay J. E., 1983, ApJ, 266, 160

Lee H., Park M., 1999, ApJL, 515, L89

Livio M., 1988, Accretion from Stellar Winds. IAU Colloq. 103: The Symbiotic Phenomenon, p. 149

Luthardt R., 1992, in Reviews of Modern Astronomy, Vol. 5, p. 38

Lyubarskii Y. E., 1997, MNRAS, 292, 679

Meyer-Hofmeister E., Schandl S., Deufel B., Barwig H., Meyer F., 1998, A&A, 331, 612

Michalitsianos A. G. et al., 1993, ApJL, 409, L53

Mikolajewska J., Kenyon S. J., 1992a, AJ, 103, 579

Mikolajewska J., Kenyon S. J., 1992b, MNRAS, 256, 177

Mikolajewski M., Mikolajewska J., 1988, An Accretor-Propeller Model of CH Cygni. IAU Colloq. 103: The Symbiotic Phenomenon, p. 233

Mikolajewski M., Mikolajewska J., Khudiakova T. N., 1990b, A&A, 235, 219

Mikolajewski M., Mikolajewska J., Tomov T., Kulesza B., Szczerba R., 1990a, Acta Astronomica, 40, 129

Muerset U., Nussbaumer H., Schmid H. M., Vogel M., 1991, A&A, 248, 458

Muerset U., Wolff B., Jordan S., 1997, A&A, 319, 201

Nussbaumer H., Vogel M., 1987, A&A, 182, 51

Paczynski B., Rudak B., 1980, A&A, 82, 349

Paczynski B., Zytkov A. N., 1978, ApJ, 222, 604

Patterson J., 1994, PASP, 106, 209

Patterson J. et al., 1998, PASP, 110, 380

Popham R., di Stefano R., 1996, in LNP Vol. 472: Supersoft X-Ray Sources, p. 65

Reiger S. H., 1963, AJ, 68, 395

Reimers D., Cassatella A., 1985, ApJ, 297, 275

Robinson K., Bode M. F., Skopal A., Ivison R. J., Meaburn J., 1994, MNRAS, 269, 1

Rodgers B., Hoard D. W., Burdullis T., Machado-Pelaez L., O'Toole M., Reed S., 1997, PASP, 109, 1093

Scargle J. D., 1982, ApJ, 263, 835

Seaquist E. R., Taylor A. R., 1990, ApJ, 349, 313

Seaquist E. R., Taylor A. R., Button S., 1984, ApJ, 284, 202

Sion E. M., Fritz M. L., McMullin J. P., Lallo M. D., 1988, AJ, 96, 251

Sion E. M., Starrfield S. G., 1994, ApJ, 421, 261

Sokoloski J. L., Bildsten L., 1999, ApJ, 517, 919

Sokoloski J. L., Bildsten L., Chornock R., Filippenko A. V., 2001a, in preparation

Sokoloski J. L., Bildsten L., Ho W., 2001b, in preparation

Tomov T., Zamanov R., Kolev D., Georgiev L., Antov A., Mikolajewski M., Esipov V., 1992, MNRAS, 258, 23

van den Heuvel E. P. J., Bhattacharya D., Nomoto K., Rappaport S. A., 1992, A&A, 262, 97

van der Klis M., 1989, "Fourier Techniques in X-Ray Timing". Timing Neutron Stars, ed. H. Ogelman & E. P. J. van den Heuvel (Dordrecht: Kluwer Press), p. 27

van Teeseling A., Reinsch K., Pakull M. W., Beuermann K., 1998, A&A, 338, 947

van Zyl L., Warner B., O'Donoghue D., Sullivan D., Pritchard J., Kemp J., 1999, Baltic Astronomy, 9, 231

Walker A. R., 1977, MNRAS, 179, 587

Warner B., 1995, "Cataclysmic variable stars". Cambridge Astrophysics Series, Cambridge, New York: Cambridge University Press, —c1995

Wickramasinghe D. T., Ferrario L., 2000, PASP, 112, 873

Willson L. A., Garnavich P., Mattei J. A., 1981, Informational Bulletin on Variable Stars, 1961, 1

Yonehara A., Mineshige S., Welsh W. F., 1997, ApJ, 486, 388

Young A. T., 1967, AJ, 72, 747

Yungelson L., Livio M., Tutukov A., Kenyon S. J., 1995, ApJ, 447, 656

Zamanov R. K., Bruch A., 1998, A&A, 338, 988

APPENDIX A: AVERAGE POWER OF POISSON NOISE WITH THE LEAHY NORMALIZATION

Using the Leahy et al. (1983) normalization, we relate the average power in the power spectrum to the rms variation of a light curve via Parseval's theorem,

$$\sum_{k=0}^{N-1} |c(k)|^2 = \frac{1}{N} \sum_{j=-N/2}^{N/2-1} |a_j|^2. \quad (\text{A1})$$

The variance of $c(k)$ is

$$\sigma^2 \equiv \frac{1}{N} \sum_{k=0}^{N-1} (c(k) - \bar{c})^2 = \overline{c^2} - \bar{c}^2. \quad (\text{A2})$$

This variance should be the same as that given by equation (9) for a single star if observations are made under ideal conditions, and airmass effects are removed from the data. Plugging in from equation (A1),

$$\sigma^2 = \overline{c^2} - (\bar{c})^2 = \frac{1}{N} \sum_{k=0}^{N-1} c(k)^2 - \left(\frac{1}{N} \sum_{k=0}^{N-1} c(k) \right)^2 \quad (\text{A3})$$

$$= \frac{1}{N^2} \sum_{j=-N/2}^{N/2-1} |a_j|^2 - \frac{1}{N^2} a_0^2 \quad (\text{A4})$$

$$= \frac{1}{N^2} \sum_{j=-N/2, j \neq 0}^{N/2-1} |a_j|^2 \quad (\text{A5})$$

$$= \frac{1}{N^2} \sum_{j=-N/2, j \neq 0}^{N/2-1} \frac{C_{tot} P_j}{2} \quad (\text{A6})$$

$$= \frac{C_{tot}}{N^2} \left(\sum_{j=1}^{N/2-1} P_j + \frac{1}{2} P_{N/2} \right), \quad (\text{A7})$$

where in the last step we used the fact that $|a_j| = |a_{-j}|$. The fractional rms variation squared is then just

$$s^2 = \frac{\sigma^2}{\bar{c}^2} = \frac{N^2 \sigma^2}{C_{tot}^2} = \frac{1}{C_{tot}} \left(\sum_{j=1}^{N/2-1} P_j + \frac{1}{2} P_{N/2} \right). \quad (\text{A8})$$

For a light curve with variations due to Poisson statistics only, we expect $s^2 = 1/\bar{c} = N/C_{tot}$. Setting the expression

for s^2 in equation (A8) equal to our previous expression for s^2 , we find

$$\frac{N}{C_{tot}} = \frac{1}{C_{tot}} \left(\sum_{j=1}^{N/2-1} P_j + \frac{1}{2} P_{N/2} \right), \quad (\text{A9})$$

or

$$\frac{2}{N} \left(\sum_{j=1}^{N/2-1} P_j + \frac{1}{2} P_{N/2} \right) = 2 \quad (\text{A10})$$

$$\Rightarrow \bar{P} = 2 + \underbrace{\frac{P_{N/2}}{N}}_{\text{small}} \approx 2, \quad (\text{A11})$$

where \bar{P} is the average power excluding the D.C. power P_0 . So, for the power spectrum of Poisson noise with this normalization, the mean value of the power at non-zero frequencies is approximately 2.

This paper has been produced using the Royal Astronomical Society/Blackwell Science L^AT_EX style file.